AD-A069 528 SRI INTERNATIONAL MENLO PARK CA F/G 7/2
NUCLEATION AND GROWTH OF CRACKS IN CVD ZNS UNDER PARTICLE IMPAC--ETC(U)
APR 79 D A SHOCKEY, K C DAO, D R CURRAN N00014-76-C-0657

UNCLASSIFIED NL

1 OF 1
AD
A069528

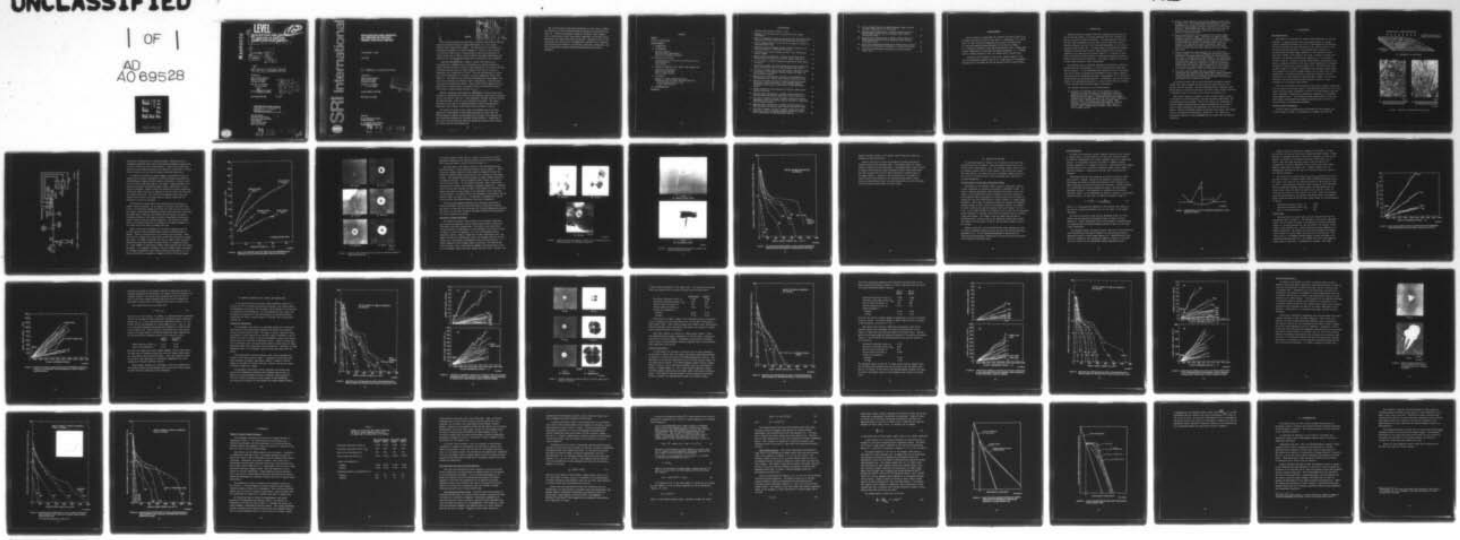

END
DATE FILMED
7-79
DDC

LEVEL II

NUCLEATION AND GROWTH OF CRACKS IN CVD ZnS UNDER PARTICLE IMPACT

Annual Report — Part II

April 1979

55 p.

By: D. A. Shockey, K. C. Dao, and D. R. Curran

Prepared for:

Office of Naval Research
800 N. Quincy Street
Arlington, VA 22203

Attn: Dr. R. C. Pohanka
Dr. A. M. Diness

Contract N00014-76-C-0657

SRI Project PYU-4928

SRI International
333 Ravenswood Avenue
Menlo Park, California 94025
(415) 326-6200
Cable: SRI INTL MNP
TWX: 910-373-1246

SRI International

NUCLEATION AND GROWTH OF CRACKS IN CVD ZnS UNDER PARTICLE IMPACT

Annual Report — Part II

April 1979

By: D. A. Shockey, K. C. Dao, and D. R. Curran

Prepared for:

Office of Naval Research
800 N. Quincy Street
Arlington, VA 22203

Attn: Dr. R. C. Pohanka
Dr. A. M. Diness

Contract N00014-76-C-0657

SRI Project PYU-4928

Approved:

G. R. Abrahamson, Director
Poulter Laboratory

P. J. Jorgensen, Vice President
Physical and Life Sciences

SUMMARY

This research program was undertaken to identify and evaluate material properties governing fracture damage development in a laser window material under hard particle impact. The approach was to determine the sequential development of fracture damage in a ceramic in the vicinity of a particle impact site, to quantitatively assess the population of radial cracks, and to deduce crack nucleation and growth expressions and properties by correlating the damage with an appropriate load parameter.

Individual 800-μm-diameter tungsten carbide (WC) spheres were accelerated in a pneumatic gun to velocities up to 80 m/s and made to impact polished surfaces of chemical-vapor-deposited zinc sulfide (CVD ZnS) to produce various levels of impact damage in the form of a plastic impression and a population of cracks. The size distributions of radial cracks were determined as a function of plastic impression radius (see Figure 7). The shapes of the crack size distribution curves suggest that the size distribution of inherent flaws is exponential, consistent with the results of probability theory. These curves further suggest that the growth law for radial cracks is similar in form to expressions derived from elastic energy balances (Section V).

Material parameters describing the development of radial cracks were obtained by correlating the crack size distributions with plastic impression strain (see Figures 9 and 10). These parameters included threshold strains and characteristic rates for crack nucleation and growth. The values obtained for the case of an 800-μm-diameter WC sphere perpendicularly impacting a flat surface of CVD ZnS are given on pages 17 and 20.

The effects of particle size, shape, and loading rate on fracture damage were investigated by performing experiments in which 400- and 800-μm-diameter tungsten carbide spheres and cylinders were impacted and quasi-statically pressed onto polished CVD ZnS surfaces. Comparison of the crack size distributions indicated significant particle size effects, but lesser effects from loading rate.

The crack nucleation and growth parameters for the cases of impacts and indents with 400- and 800-μm-diameter spheres were determined (see Table 1). Several discrepancies among the parameter values suggest that a load parameter other than plastic impression strain may be more appropriate for extracting erosion properties. Research efforts in the coming year will make use of the damage data reported here to identify more suitable load parameters, attain more consistent correlations, and seek relationships between standard macroproperties and erosion parameters.

CONTENTS

ILLUSTRATIONS

ACKNOWLEDGMENTS

We are pleased to acknowledge the interest and help of many of our colleagues during the course of this work: K. Hirschberg, R. W. Gates and L. B. Hall assisted in designing the particle accelerator and D. Petro made numerous photomicrographs of the fracture damage. D. J. Rowcliffe examined the CVD ZnS microstructure, and L. Seaman made helpful suggestions for obtaining the damage parameters. S. L. McHugh wrote a computer program to plot the copious data in various ways.

A special debt of thanks is owed to Mr. Lawrence Kopell of the Air Force Materials Laboratory and to Dr. James Pappis of the Raytheon Corporation for providing the CVD ZnS material used in these studies.

I INTRODUCTION

Materials having acceptable radiation transmission properties for use as infrared windows on aircraft generally have poor resistance to fracture in particle impact situations. The microfractures that form and grow under bombardment by rain, dust, and ice particles scatter incident radiation and result in continuous degradation of the optical properties with flight time. The Navy wishes to establish more impact-resistant microstructural forms of these materials and to develop a capability for predicting the fracture behavior. In support of these needs, the Office of Naval Research is sponsoring research programs at several universities and institutes. This report summarizes the status of work being performed at SRI International.

Our objective was to establish expressions and material properties governing fracture development in a laser window material under hard particle impact. If such expressions and properties can be established, they can be useful in guiding the development of more impact resistant microstructures by permitting systematic investigation of the effects of compositional and processing variables. Furthermore, they can be used to predict such engineering quantities as optical and mechanical lifetimes of laser windows under specified impact environments.

Our approach consisted of the following tasks:

- Establish an experiment that can be analyzed to allow identification and evaluation of the material properties governing resistance of semibrittle materials to fracture damage by particle impact. Experiments having the highest probability of success appeared to be those closely simulating particle impact conditions, but having a simple impact geometry to aid in interpretation and analysis. Thus, we performed experiments involving normal (90°) impact of a single, elastic, submillimeter-diameter sphere against a flat specimen surface.

- Obtain an understanding of how fracture damage develops about an impact site. We studied damage phenomenology by performing experiments at various velocities so as to produce various levels of damage ranging from below incipient to surface fragmentation. By examining the impact sites and cross sections taken through the sites with a microscope we deduced the history of damage development.
- Describe quantitatively the deformation and fracture damage produced by particle impact. Definition of impact erosion properties requires a knowledge of the relationships between loading parameters and material failure response, and therefore a quantitative description of deformation and fracture is required. We measured the plastic impression radius and counted and measured the radial cracks at particle impact sites to obtain crack size distributions for various impact velocities.
- Choose an appropriate load parameter for correlation with fracture damage. To extract fundamental and general material properties, the damage quantities should be correlated with the stress or strain histories experienced at the appropriate locations in the impacted specimen. However, the determination of stress and strain as a function of location and time is a complicated and difficult problem for a material undergoing plastic flow and fracture, and was deferred for future work. In this work, we chose a simpler measure of the load, namely, the plastic impression strain, for correlation with damage.
- Correlate fracture damage with load parameter to extract expressions and properties describing impact damage development. The numbers and sizes of radial cracks were correlated with plastic impression strain to obtain expressions and properties describing crack nucleation and growth.

In conducting these tasks we accelerated 800-μm-diameter tungsten carbide (WC) spheres against polished chemical-vapor-deposited zinc sulfide (CVD ZnS) surfaces. We also performed similar experiments with 400-μm spheres, cylindrical particles, and under static loading conditions to determine effects of particle size, shape, and loading rate.

This report reviews the progress in this research program. Section II describes the CVD ZnS material, the particle impact experiments, and the resulting fracture damage. Section III deduces the development of fracture damage caused by particle impact and describes the procedure used to obtain expressions and properties for crack nucleation and growth. Section IV examines effects of particle size, shape, and loading rate on the properties identified in Section III. The results are discussed in Section V, and recommendations for future work are given in Section VI.

II EXPERIMENTAL

Specimen Material

Experiments were performed on chemical-vapor-deposited zinc sulfide (CVD ZnS). A half-inch-thick slab of material produced in an AFML research program was provided to us by Dr. James Pappis of the Raytheon Corporation through the kind cooperation of Mr. Lawrence Kopell of the Air Force Materials Laboratory. The microstructure consisted of columnar grains oriented roughly parallel to the direction of vapor deposition (normal to the plane of the plate), as shown in Figure 1(a). The grains had average cross-sectional diameters of 7 μm and aspect ratios of about 8. Colonies of grains having similar orientations were joined to adjacent colonies by low angle colony boundaries that extended through the thickness of the slab, Figure 1(c). The material was theoretically dense at 4.08 g/cm^3; longitudinal and transverse sound speeds were measured by the time-of-flight method to be 5.4 mm/μs and 3.2 mm/μs, respectively. No inherent defects or flaws that might act as crack initiation sites were obvious at magnifications to 1000x. We speculate therefore that internal fractures may nucleate at grain or colony boundaries or at boundary triple points.

The slab was machined into round disks and rings of several thicknesses with the plane of the plates normal to the deposition direction, Figure 1(a), for use in plate impact experiments (see Part I of this report), particle impact experiments, quasi-static indentation experiments, and expanded-ring toughness tests.[1] The estimated surface finish was 0.8 μm for the plate impact and expanded-ring toughness specimens and 0.2 μm for the particle impact and indentation specimens.

Particle Impact Experiments

Particle impact experiments were performed with the pneumatic gun facility shown in Figure 2, consisting of a cylinder that could be

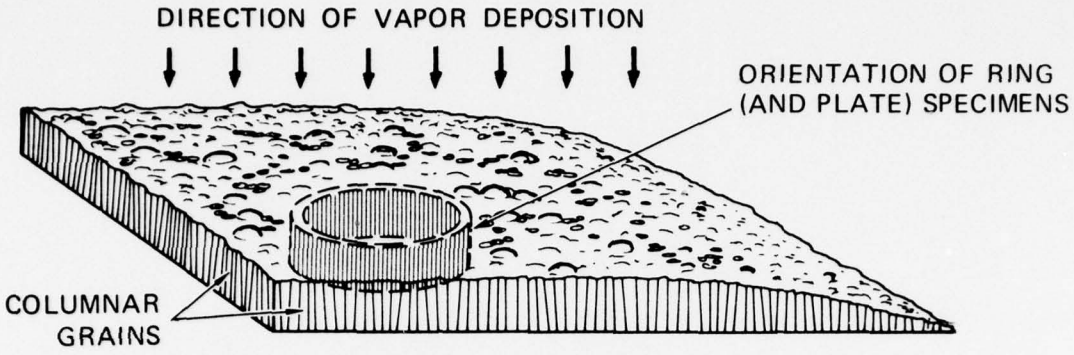

(a) SCHEMATIC OF ZnS PLATE

(b) GRAIN STRUCTURE AS VIEWED IN DEPOSITION DIRECTION

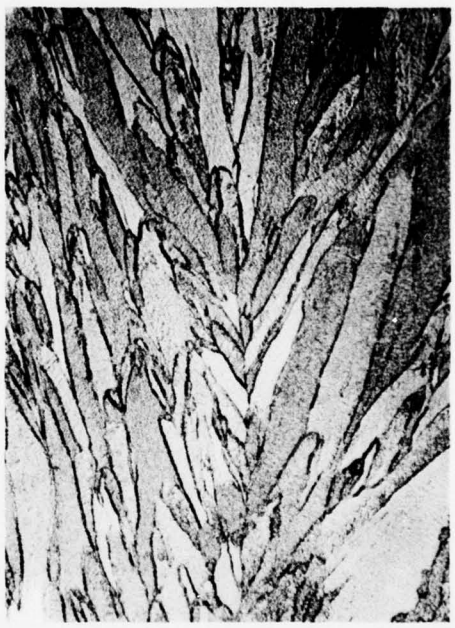

(c) GRAIN STRUCTURE NORMAL TO DEPOSITION DIRECTION

MP-4928-2

FIGURE 1 CHEMICAL-VAPOR-DEPOSITED PLATE OF ZnS

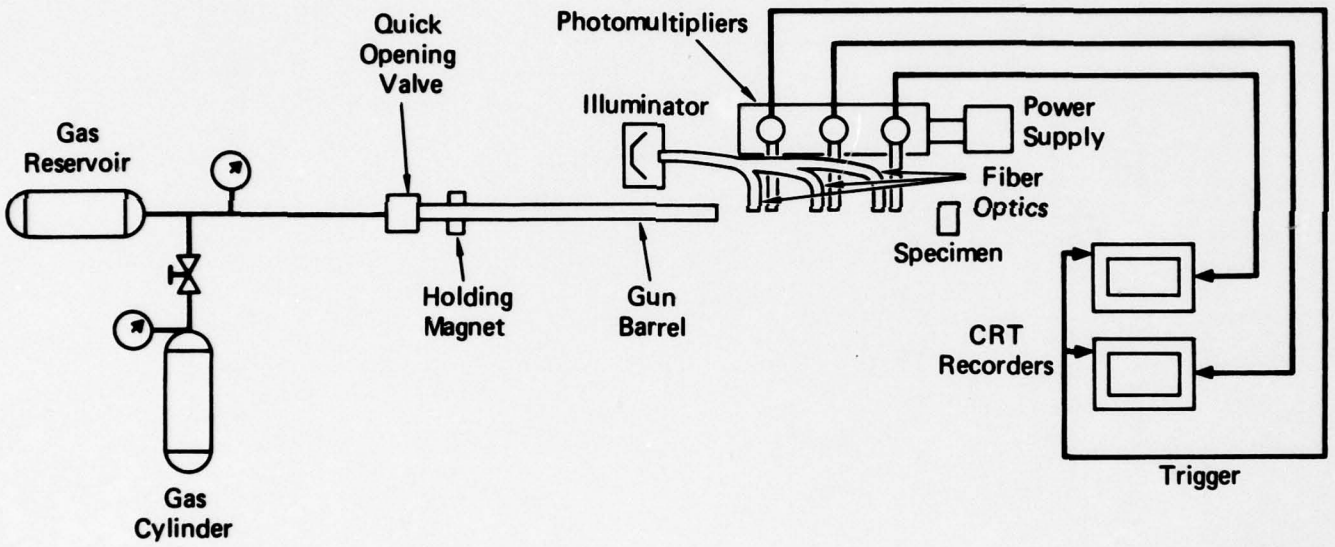

FIGURE 2 SCHEMATIC OF PNEUMATIC GUN FACILITY USED TO PERFORM PARTICLE IMPACT EXPERIMENTS

filled with nitrogen gas to a desired pressure, 150-mm-long interchangeable stainless steel tubes having internal diameters ranging from 0.48 to 1.06 mm, and a quick opening valve. Particle velocities were measured by three photomultipliers that received a light pulse reflected from the particle as the particle passed three known positions.

To study the evolution of impact damage, we performed a series of single-particle impact experiments on CVD ZnS surfaces using 800- and 400-μm-diameter tungsten carbide spheres accelerated to various velocities up to 80 m/s and impacting at a 90° angle. Impacting spheres of a given size produced successively larger plastic impressions as their velocity increased. Figure 3 shows the variation in plastic impression radius with impact velocity for spheres of the two sizes, and also shows the rebound velocities. The curves for the smaller sphere rise less sharply than those for the larger sphere, possibly reflecting the difference in radii of curvature.

The difference between impact and rebound velocity increases as impact velocity increases. At low impact velocities (less than about 10 m/s), the particles rebound with nearly the same velocity with which they impact, indicating predominantly elastic particle/target interaction. At higher impact velocites, the rebound velocity becomes a steadily decreasing fraction of the impact velocity, indicating increasing nonelastic (plastic flow and fracture) behavior. The difference between impact and rebound velocities is a measure of the momentum imparted to the target and can be used to estimate the load.

Figure 4 shows the development of the plastic impression and the fracture pattern with increasing impact velocity of 800-μm-diameter spheres. Below a certain velocity, no fractures were observed. Above that velocity, usually five large radial cracks were produced in a spoke-like array. At higher velocities, the size of larger cracks increased significantly and their number increased slowly to a maximum of about 10. Large numbers of much smaller radial cracks appeared near the contact periphery. It is apparent in Figure 4 that the radial cracks are present in a bimodal distribution, each fracture pattern consisting of 5 to 10 radial cracks 300 μm or greater in length, and 30 to 50 cracks having

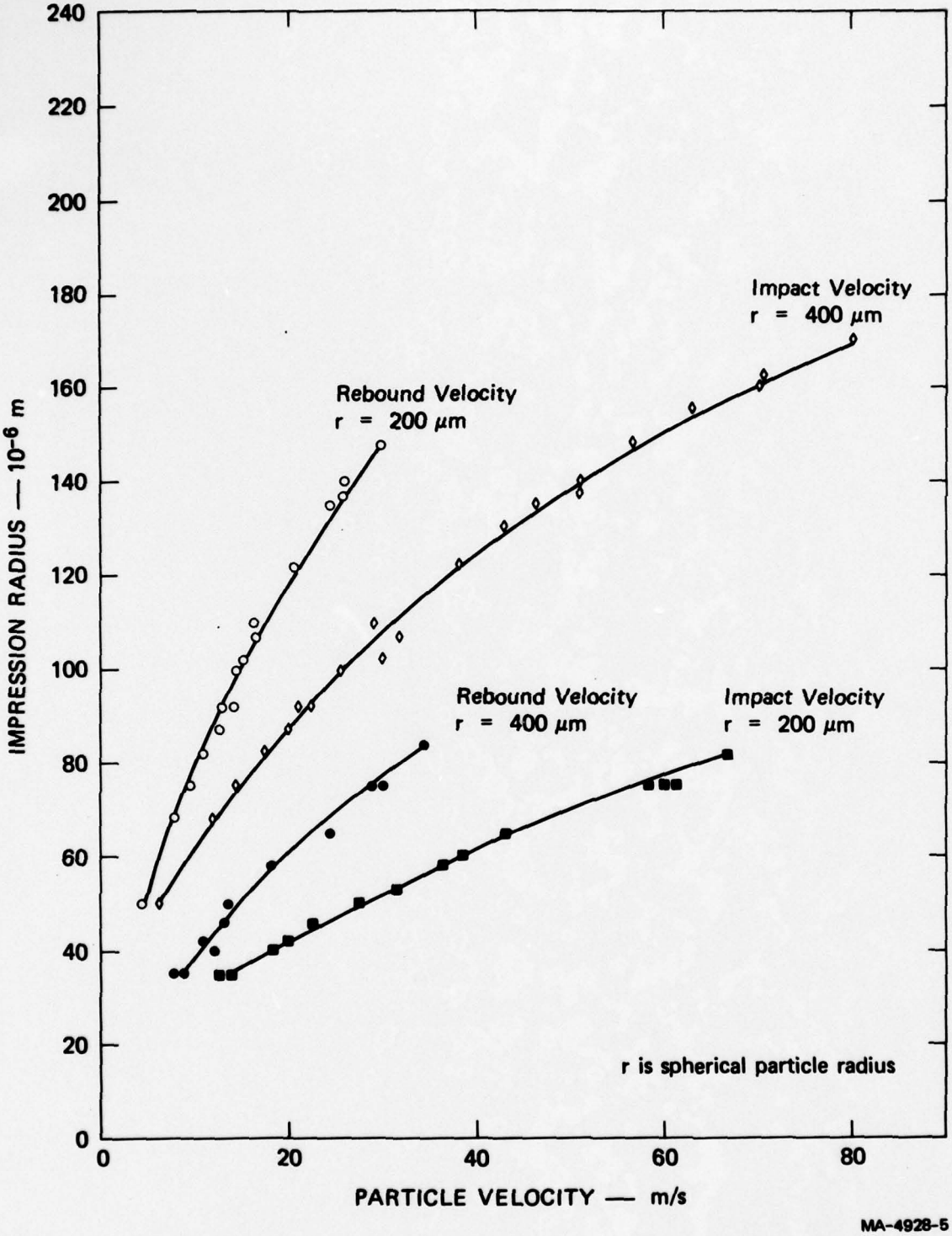

FIGURE 3 IMPACT AND REBOUND VELOCITIES ASSOCIATED WITH IMPRESSION RADII PRODUCED IN CVD ZnS BY 800 AND 400-μm-DIAMETER WC SPHERES

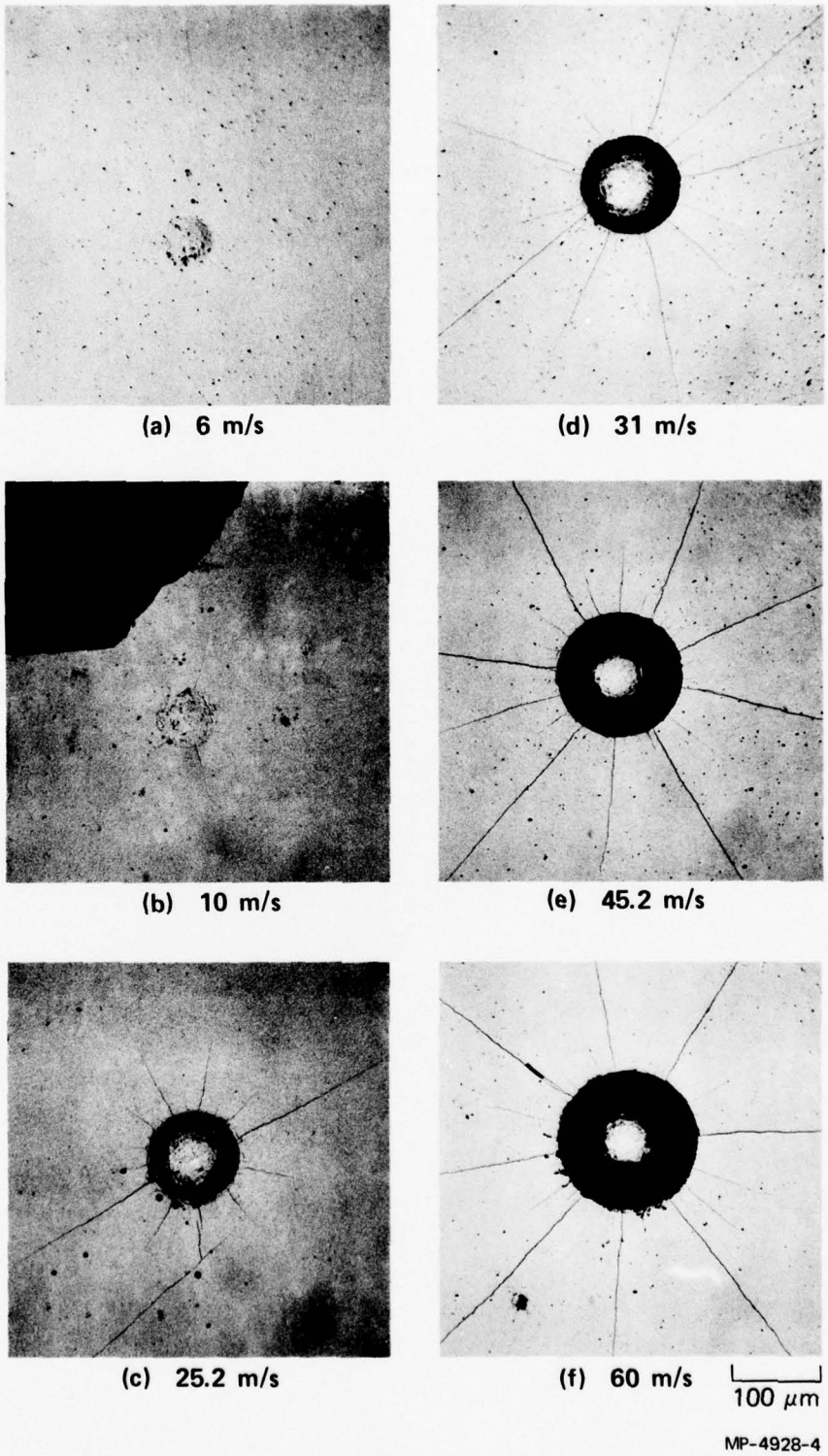

FIGURE 4 SURFACE DAMAGE PRODUCED IN CVD ZnS BY AN IMPACTING SPHERE AT INCREASING VELOCITIES

an average length of about 100 μm. Figure 4 also shows the plastic impression produced by the impacting sphere and its monotonic growth with increasing impact velocity (see also Figure 3).

The same impact sites shown in Figure 4 were photographed using polarized light to reveal subsurface lateral cracks, Figure 5. These cracks lay roughly parallel to and beneath the impacted surface and formed at somewhat higher velocities than were required to form radial cracks: they propagated radially outward on planes roughly parallel to the impacted surface. Like the dominant radial cracks, less than 10 lateral cracks formed. At the higher velocities, these cracks often intersected the surface and liberated a fragment, Figure 5(c). Polished cross sections taken through the impact sites showed the profiles of the radial and lateral cracks, Figure 6, and revealed a third crack type (called median). The median cracks are orthogonal to the surface and lie directly under the impact site. In addition, a hemispherical zone of porous material was observed beneath the plastic impression.

These fracture damage observations are consistent with those of Evans and Wilshaw,[2] who described the results in qualitative detail. Our intent in this work was to describe the fracture damage quantitatively and then to use the data to deduce descriptive equations and properties for crack nucleation and growth.

Quantitative Damage Assessment

The radial and lateral cracks produced in each impact experiment were counted and measured, and the results were plotted to obtain the cumulative crack size distributions. The radial crack distribution curves obtained for experiments at seven different velocities are shown in Figure 7, where the parameter, a, is the corresponding plastic impression radius. Figure 7 shows that at small impression radii (low impact velocity) the distribution curves are straight lines in the log-linear space, indicating an exponential crack size distribution. At larger impression radii (higher impact velocities), the distribution curves develop a knee, reflecting the bimodal size distribution as the 8 to 10 dominant radials grow much larger than the others. However, the

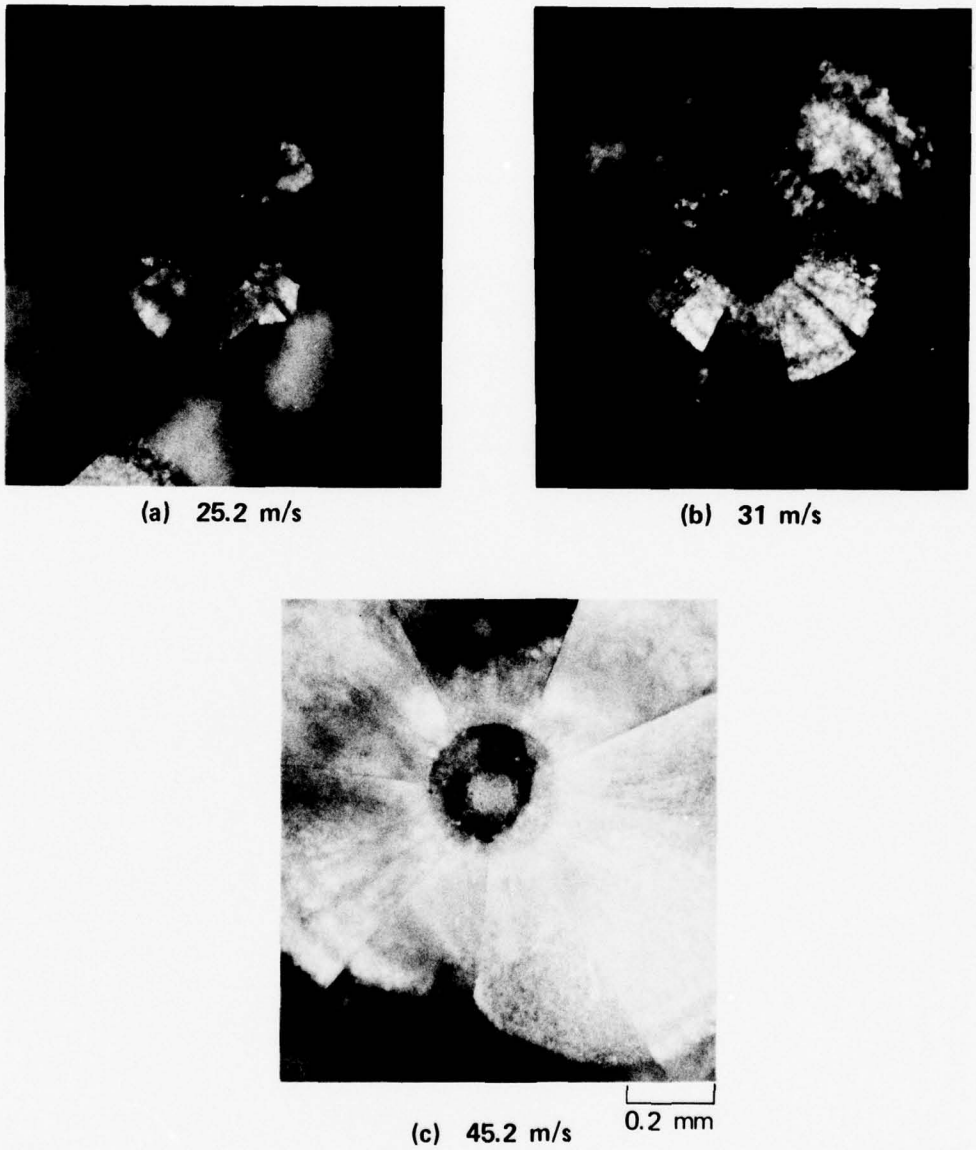

FIGURE 5 SUBSURFACE FRACTURE DAMAGE (LATERAL CRACKS) PRODUCED BY AN IMPACTING SPHERE AT INCREASING VELOCITIES

(a) BRIGHT FIELD LIGHT

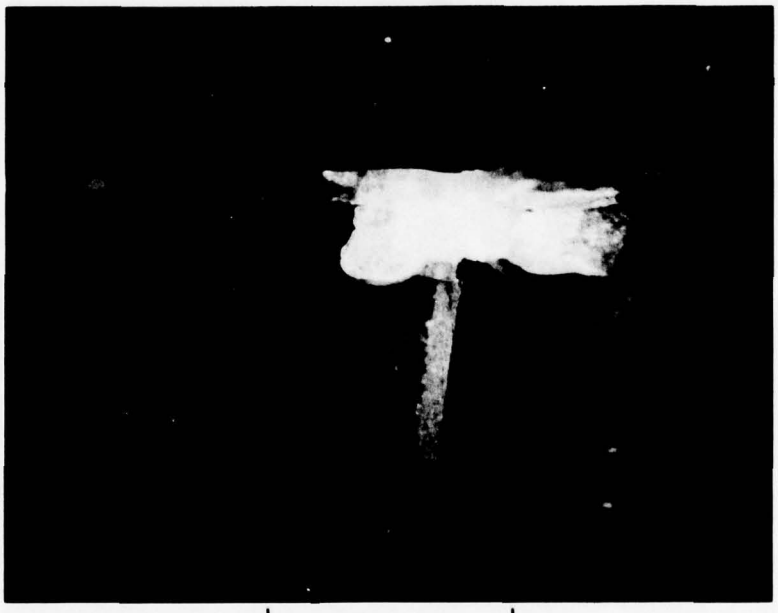

(b) POLARIZED LIGHT

MP-4928-7

FIGURE 6 POLISHED CROSS SECTION THROUGH AN IMPACT SITE SHOWING SUBSURFACE DAMAGE

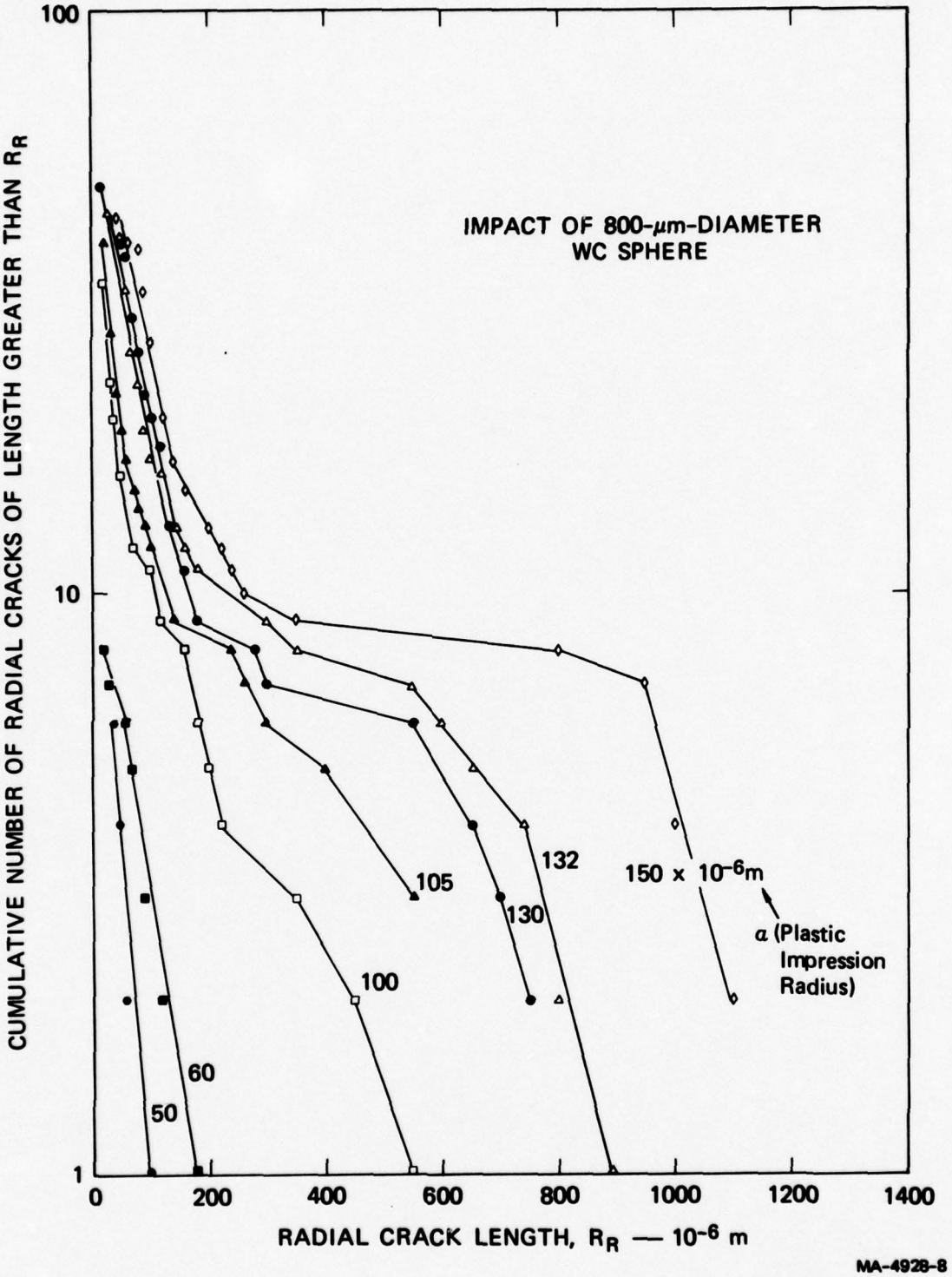

FIGURE 7 MEASURED SIZE DISTRIBUTIONS OF RADIAL CRACKS PRODUCED BY 800-μm-DIAMETER WC SPHERES AT VARIOUS IMPACT VELOCITIES

dominant radials as well as the smaller radials maintain roughly an exponential size distribution.

Lateral cracks were counted and measured by viewing through the specimen surface with polarized light. The maximum number of lateral cracks we observed by this method was 6, although polished cross sections of impact sites revealed several additional lateral cracks lying above the main laterals that were not easily detected by viewing normal to the impact surface. Because of the uncertainties in the number of lateral cracks as determined by the polarized light method, lateral crack size distribution curves are not presented here, and the following fracture analysis concentrates on radial cracks.

III ANALYSIS OF THE DATA

The photomicrographs of Figure 4 and the shapes of the crack size distribution curves in Figure 7 show that radial cracks exist in two rather distinct size groups: the 5 to 10 largest cracks, which we call the dominant radials, and all other radials, which never grow larger than about 200 μm. We treat here only the dominant radials since they are the first to form and since they are probably most important in strength degradation.

Interpretation of Crack Size Distribution Curves

Development of the dominant radial cracks is considered a kinetic process consisting of nucleation and growth of individual cracks. To extract equations describing crack nucleation and growth, we view the family of size distribution curves in Figure 7 not as the results of seven separate impact experiments at various velocities, but rather as giving the crack size distribution at various stages of a single impact experiment. Thus, when the impacting sphere has produced an impression having a radius of 50 μm, there are six dominant radials, the largest of which is 100 μm long and the smallest (the sixth largest) is 40 μm long. As the sphere continues to penetrate into the ZnS and the impression radius continues to increase, more cracks are produced and the existing cracks grow larger. For example, when the sphere has produced an impression with a radius of 60 μm, two additional radials have formed, the largest crack has grown to 180 μm, and the sixth largest crack is 60 μm long.

Viewed in this way, the size distribution curves indicate the rate at which the dominant radials nucleate and grow with increasing plastic impression size. In the following paragraphs we demonstrate how expressions and parameters (properties) for crack nucleation and growth can be extracted from these data.

Crack Nucleation

As noted in the previous section, dominant radials are not created by impacts below a certain velocity, but when that critical velocity is attained, approximately five radials suddenly appear in a spoke-like pattern. At increasing velocities the number of dominant radials increases gradually to a maximum of about ten. These observations suggest several properties for nucleation of dominant radial cracks, namely, a threshold condition, a saturation condition, and a nucleation rate parameter.

These properties are best expressed in terms of stress or strain field history. However, because of the difficulty associated with determining the stress or strain field history in the vicinity of an impact when plastic flow and fracture are occurring, a simpler parameter for correlations with fracture damage was sought. We chose plastic impression strain Q. This expression is obtained from the plastic impression radius, a, by considering the change in length of a plastically indented surface. For the case of a spherical indenter, Figure 8,

$$Q = \ln \frac{r\theta}{a} = - \ln \frac{a/r}{\text{arc sin } a/r} \qquad (1)$$

where r is a characteristic dimension of the particle (the radius in the case of a spherical particle) and a is the radius of the plastic impression.

We noted in Section II that plastic impression radius is a well defined and monotonically increasing function of impact velocity (Figure 3). Plastic impression strain also provides a convenient basis for comparing particle-induced damage produced by impact and by quasi-static indentation.

The threshold strain, saturation strain, and rate of crack nucleation were determined from the data of Figure 7 by converting the plastic impression radius to strain using equation (1), choosing several crack sizes for evaluation, and plotting the number of cracks of a selected size as a function of the appropriate plastic impression strain.

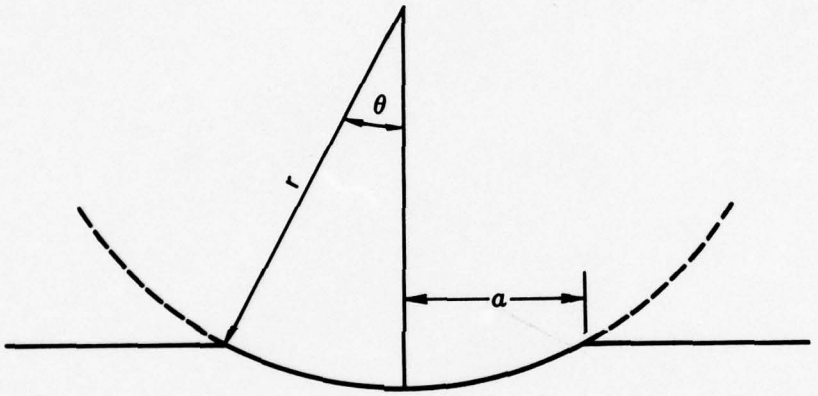

FIGURE 8 CROSS SECTION OF PLASTIC IMPRESSION PRODUCED BY RIGID SPHERE OF RADIUS *r*

Figure 9 gives the results for radials of four sizes: 40, 100, 300, and 400 μm. The last two sizes represent dominant radials. Extrapolations of straight-line fits to the curves converge at a point on the abscissa and indicate a well-defined intercept strain value Q_i of 0.0018. Note that this intercept strain is not the same as the "engineering" nucleation threshold strain at which five radial cracks suddenly appear about the impact site. However, because it is so unambiguously indicated by the data, the intercept strain was taken as the material parameter.

The slopes of the curves labeled N_{300} and N_{400} indicate the rate of increase in number of dominant radials with increasing impression strain. The slope of the curve for the 400-μm-long crack is 390 cracks per unit of strain. The saturation strain for crack nucleation (the strain above which no additional dominant radials appear) was determined from the curves as the strain for which ten cracks occur, that is, 0.028. We estimated the scatter in these values to be $\pm$ 30%. Thus, the following three quantities describe the observed nucleation behavior of dominant radial cracks produced in CVD ZnS under normal impact by a 800-μm-diameter WC sphere.

Nucleation intercept strain, Q_i	0.18%
Nucleation saturation strain, Q_{sat}	2.8%
Rate of crack nucleation, B	390

Crack Growth

The growth law for radial cracks was also obtained from the size distribution data in Figure 7. The parameter a, the plastic impression radius, for the curves in Figure 7 was converted to plastic impression strain Q by using equation (1), and the sizes of the largest, second largest, third largest, etc., radial cracks were plotted against Q, as shown in Figure 10. The family of curves results because the dominant radial cracks for a given impact event are not of uniform size. Thus each of the 5 to 10 dominant radials appears to grow according to its individual characteristic rate. We consider only two of the family of growth rates in this work: a maximum and an average. The former

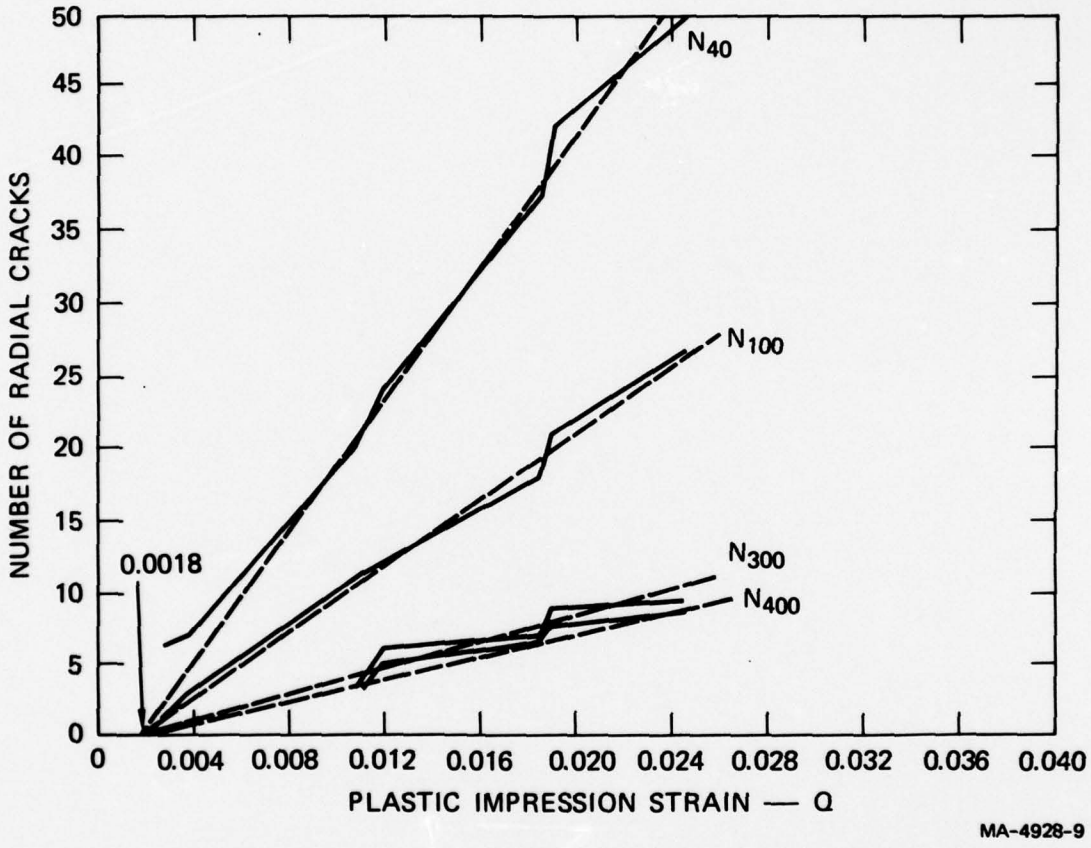

FIGURE 9 VARIATION OF NUMBER OF RADIAL CRACKS WITH PLASTIC IMPRESSION STRAIN PRODUCED BY IMPACT OF 800-μm -DIAMETER WC SPHERES

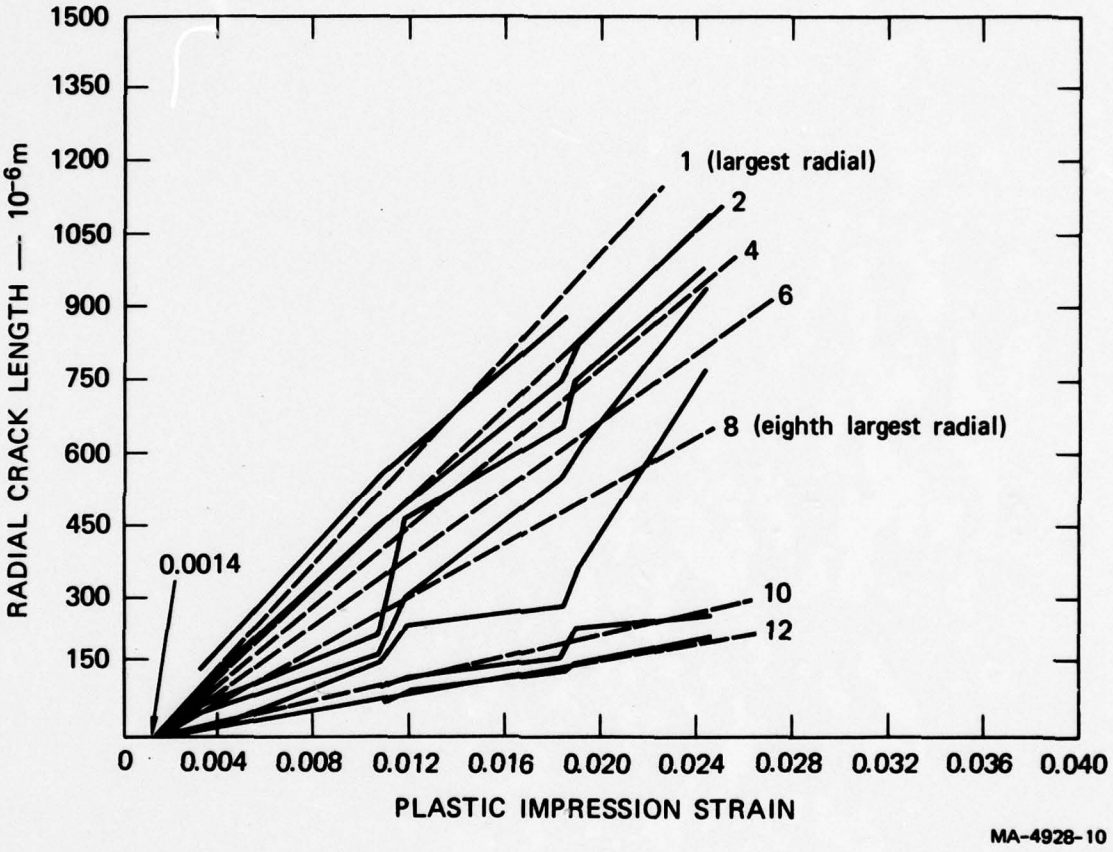

FIGURE 10 VARIATION OF RADIAL CRACK SIZE WITH PLASTIC IMPRESSION STRAIN FOR SEVERAL OF THE DOMINANT RADIALS PRODUCED BY IMPACT OF 800-μm — DIAMETER SPHERES

describes the growth of the largest crack and is important because, in strength degradation considerations, the largest crack may determine the residual strength. The second growth equation describes the growth rate of the fourth largest dominant radial and as such indicates an approximate average size of the damaged region about an impact site.

Both growth rates have the simple form

$$R = b(Q - Q_o) \qquad (2)$$

where R is the crack length, $b = dR/dQ$ is a growth parameter expressing the rate of increase in crack length with increasing plastic impression strain, and Q_o is the intercept plastic impression strain, i.e., the plastic strain corresponding to a crack length of zero. Thus Q_o and b are material parameters describing the propagation of radial cracks from an impact site. Their values for the largest and fourth largest radials for normal impact of an 800-μm-diameter WC sphere against CVD ZnS are given below (estimated scatter in the values is ± 30%).

	Largest Radial	4th Largest Radial
Growth intercept strain, Q_o	0.14%	0.14%
Growth rate parameter, b	54 mm	42 mm

Note that the largest and fourth largest dominant radial cracks grow at the same value of intercept strain, but that the largest radial grows at a rate faster than the fourth largest. Also, the intercept strain for growth is less than that for nucleation, suggesting that crack nucleation is the more difficult process.

These values, equation (2), and Figure 3 allow the computation of the average rosette size and maximum radial crack size from the impact velocity under the conditions of the experiment.

IV EFFECTS OF PARTICLE SIZE, SHAPE, AND LOADING RATE

If the crack nucleation and growth (NAG) parameters reported in Section III are to be taken as material properties, their values should be independent of particle size and shape, but may depend on such factors as loading rate and temperature. We investigated the size, shape, and loading rate sensitivity of the NAG parameters by performing similar experiments but using a smaller sphere, a cylinder, and a quasi-static loading rate.

Indentation Experiments

To investigate rate effects, we performed quasi-static indentation experiments, slowly pushing 800-μm-diameter WC spheres into specimen surfaces using a range of loads. The range of plastic impression sizes was similar to that produced in the particle impact experiments, and the numbers and sizes of radial cracks were determined to obtain size distribution curves as a function of impression radius. Figure 11 shows that, as in the dynamic case, the small radials (and the large radials at small impression radii) have exponential size distributions. Moreover, at large impression radii 5 to 10 dominant radials become much larger than the others.

Thus qualitatively fracture behavior under static indentation is similar to that under particle impact. Comparison of these data with those obtained from impact experiments (Figure 7) showed no obvious change in the number of radials produced; however, the size of cracks produced by impact were larger.

The parameters describing fracture nucleation and growth under quasi-static indentation conditions were obtained from the data in Figure 11 by plotting number and size of dominant radial cracks as a function of plastic impression strain, Figure 12 and determining the slopes and intercepts for the largest and average dominant radial

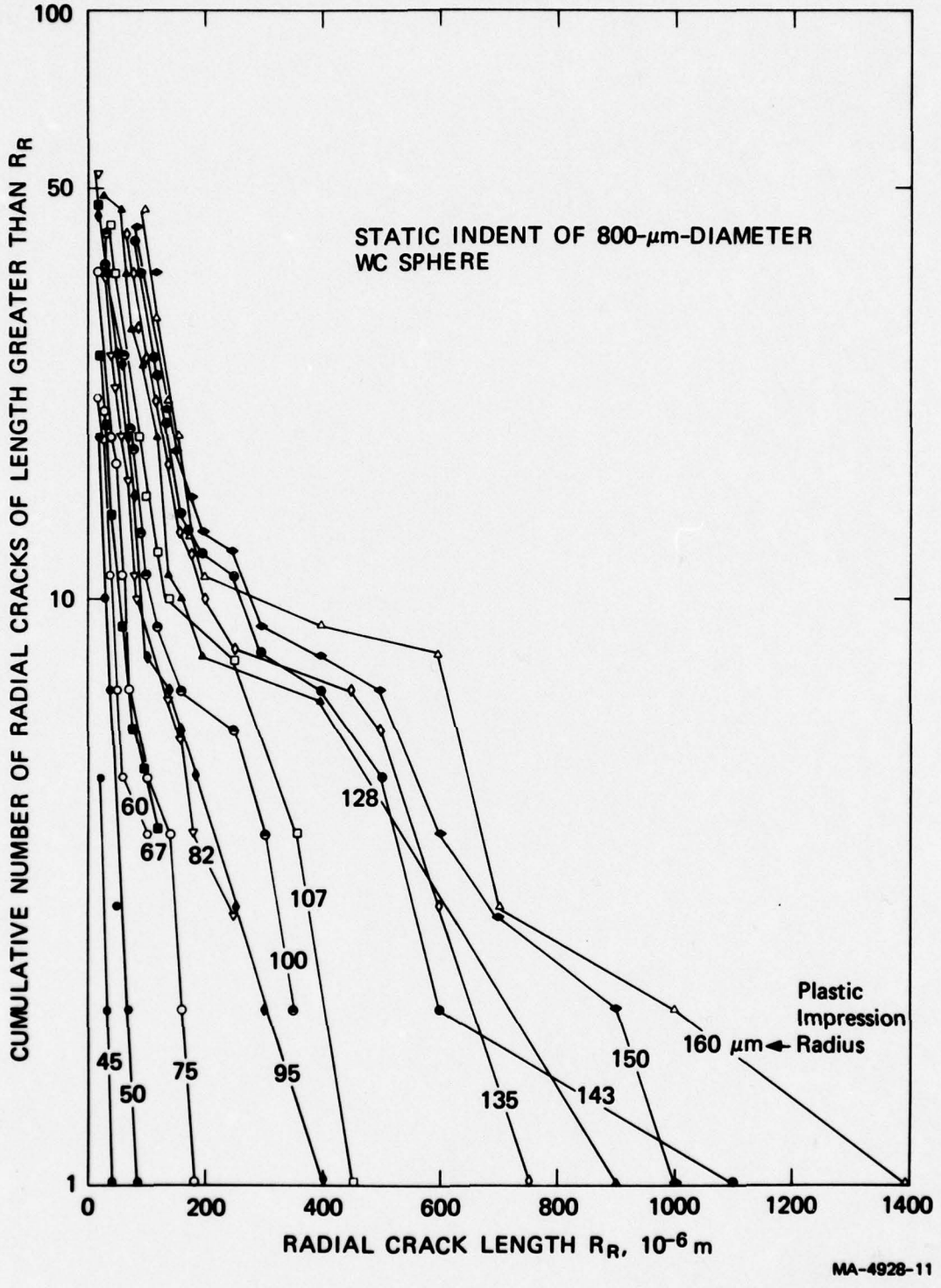

FIGURE 11 MEASURED SIZE DISTRIBUTIONS OF RADIAL CRACKS PRODUCED BY 800-μm-DIAMETER WC SPHERES UNDER VARIOUS INDENTATION LOADS

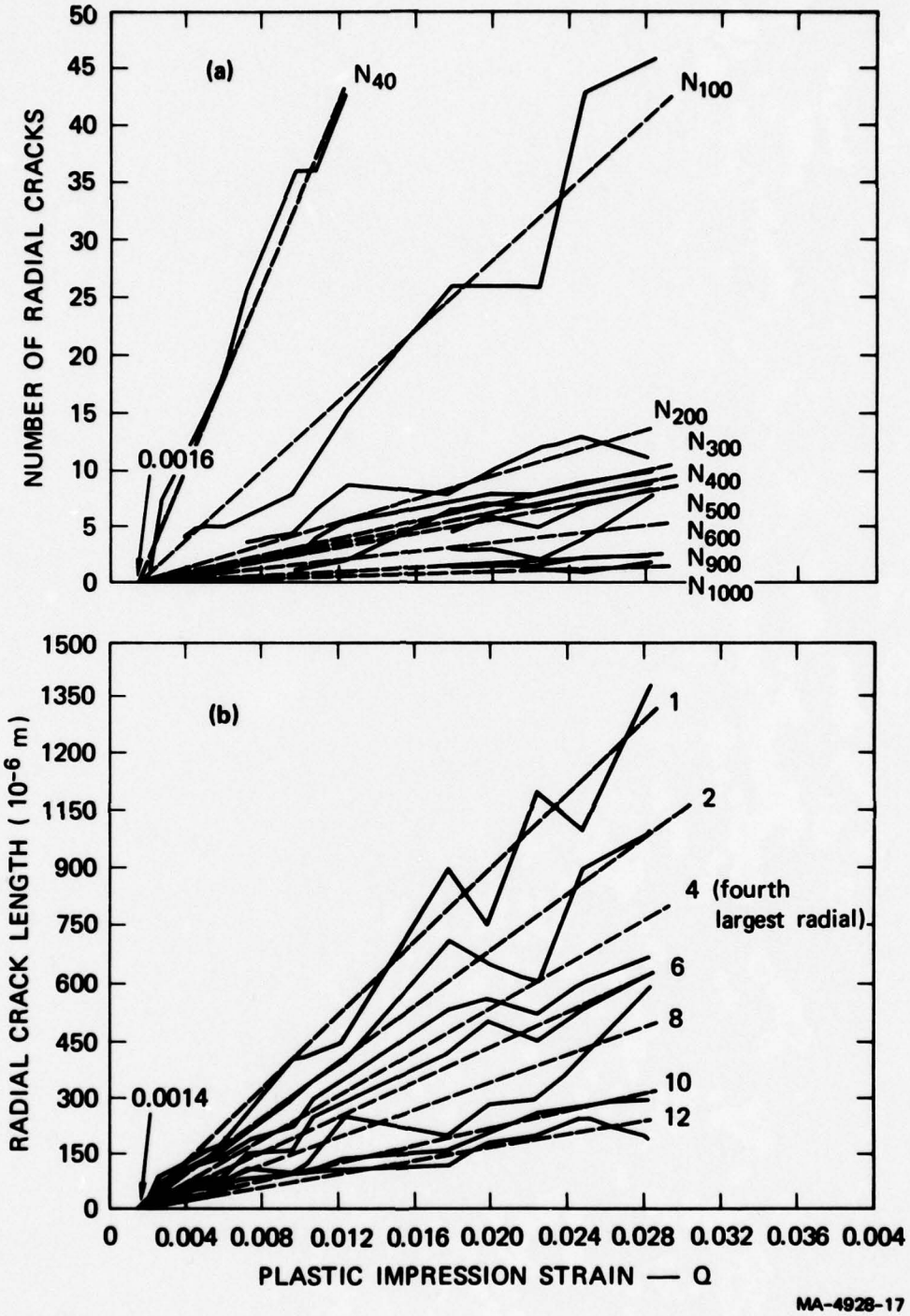

FIGURE 12 VARIATION OF NUMBER (a) AND SIZE (b) OF RADIAL CRACKS WITH PLASTIC IMPRESSION STRAIN FOR SEVERAL OF THE DOMINANT RADIALS PRODUCED BY QUASI-STATIC INDENTATIONS OF 800-μm-DIAMETER SPHERES

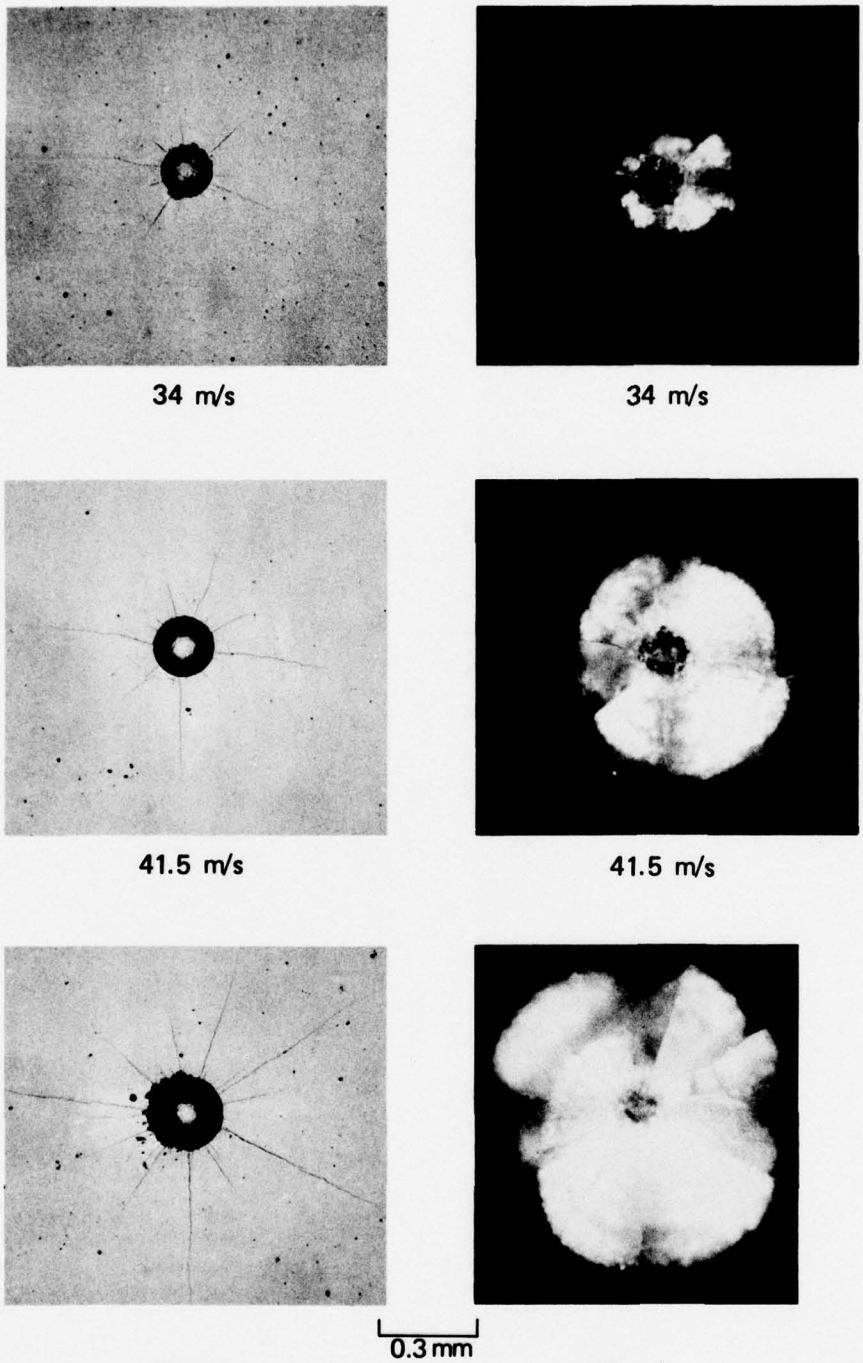

FIGURE 13 DAMAGE PRODUCED BY 400-μm-DIAMETER WC SPHERE IMPACTING AT SEVERAL VELOCITIES

cracks as done previously for the impact data. The values are presented below and compared with the values obtained from the impact data.

	Quasi-static	Dynamic
Nucleation intercept strain, Q_i	0.16%	0.18%
Nucleation saturation strain, Q_{sat}	2.8%	2.8%
Rate of crack nucleation, B	380	390
Growth intercept strain, Q_o	0.14%	0.14%
Growth rate parameters, b		
Maximum	48 mm	54 mm
Average	29 mm	42 mm

Rate effects are small: Radial crack nucleation seems to be insensitive to loading rate, and crack growth rate is only 10% to 30% greater under impact loads. These results suggest that simpler, more interpretable, and less expensive static indentation experiments can be used to evaluate impact fracture behavior of ceramics.

More work, however, is required to confirm these results. Evans and Wilshaw[3] performed similar experiments in ZnS and noted a significant rate effect on fracture damage. Furthermore, quasi-static and dynamic results based on 400-μm-diameter spheres (reported later in this section) show significant rate effects.

Particle Size Effects

To investigate the influence of particle size on these parameters, we performed a similar series of impact experiments using 400-μm-diameter WC spheres to compare with results from 800-μm-diameter WC spheres. The appearance of the plastic impression and the fracture pattern, Figure 13, was qualitatively similar to the 800-μm-diameter sphere results (compare Figures 4 and 5), as were the measured radial crack size distributions, Figure 14 (compare Figure 7). For a given plastic impression radius, the 400-μm sphere produced more and larger radial cracks than the 800-μm sphere. This might be expected because a 400-μm sphere must penetrate further to produce the same impression radius as an 800-μm sphere.

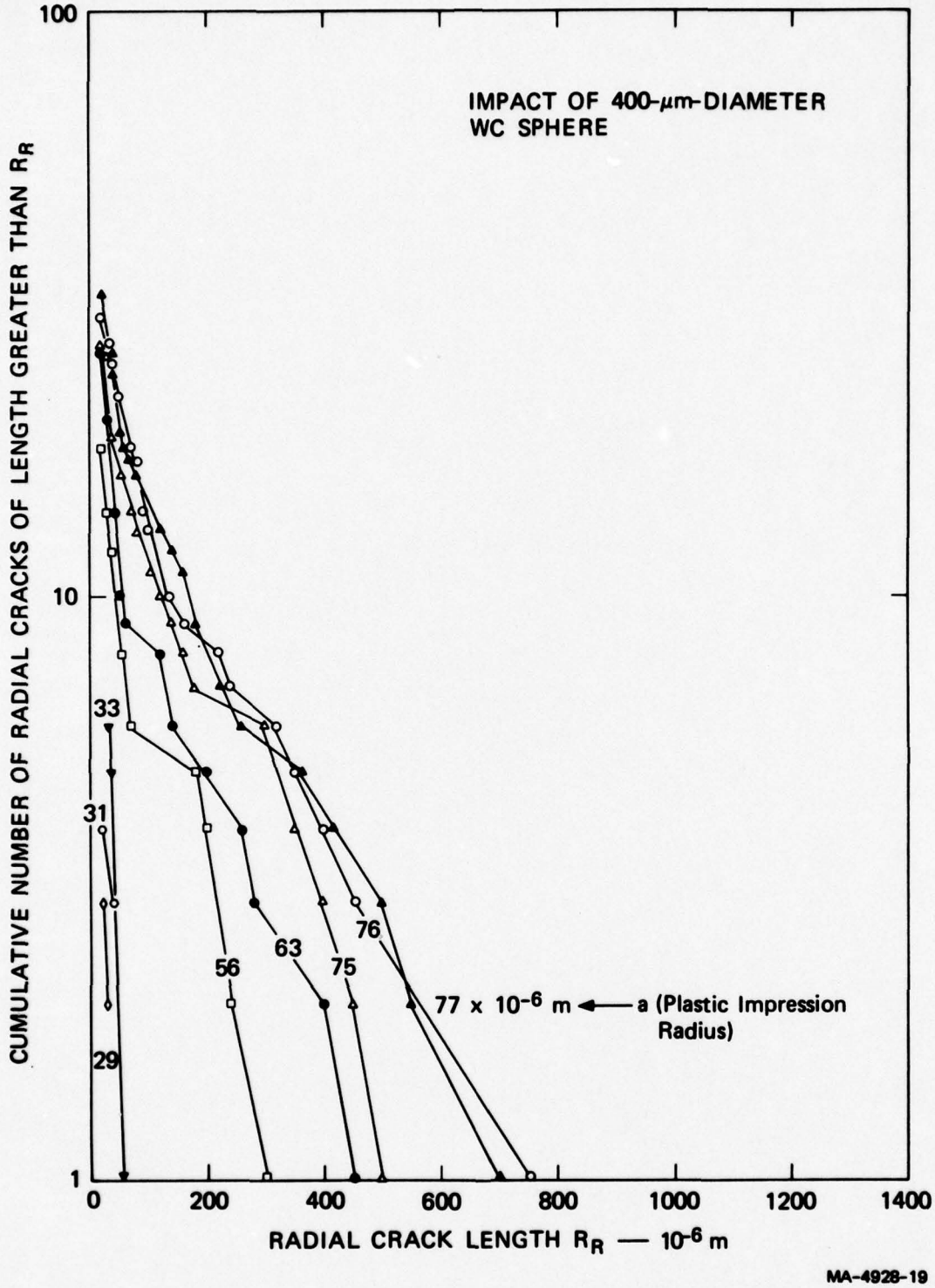

FIGURE 14 MEASURED SIZE DISTRIBUTIONS OF RADIAL CRACKS PRODUCED BY 400-μm-DIAMETER WC SPHERES IMPACTING AT VARIOUS VELOCITIES

Nucleation and growth parameters were extracted from these data in the manner described previously, Figure 15, and are compared below with those from impacting 800-μm-diameter spheres.

	400-μm Sphere	800-μm Sphere
Nucleation intercept strain, Q_i	0.20%	0.18%
Nucleation saturation strain, Q_{sat}	7.8%	2.8%
Rate of crack nucleation, B	130	390
Growth intercept strain, Q_o	0.26	0.14
Growth parameter, b		
Maximum	27 mm	54 mm
Average	17 mm	42 mm

Particle size effect on impact damage is significant in all but nucleation intercept strain: the twofold change in sphere radius results in changes in NAG parameters of factors of 2 to 3.

When quasi-static particle indentation experiments using 400-μm-diameter spheres were performed, the crack size distribution curves, Figure 16, again were qualitatively similar to previous curves. However, when the resulting damage was assessed according to the previous procedures, Figure 17, the nucleation and growth parameters were grossly different as shown below.

Nucleation intercept strain, Q_i	0.75%
Nucleation saturation strain, Q_{sat}	8.8%
Rate of crack nucleation, B	120
Growth intercept strain, Q_o	0,68%
Growth rate parameters	
Maximum	12 mm
Average	8 mm

The threshold plastic strain was 2.5 times larger than the dynamic value, and the growth rate parameter was half as large as for the impact case. This is in contrast to the case for the 800-μm-diameter spheres, for which the static and dynamic values of both parameters were found to be nearly equal.

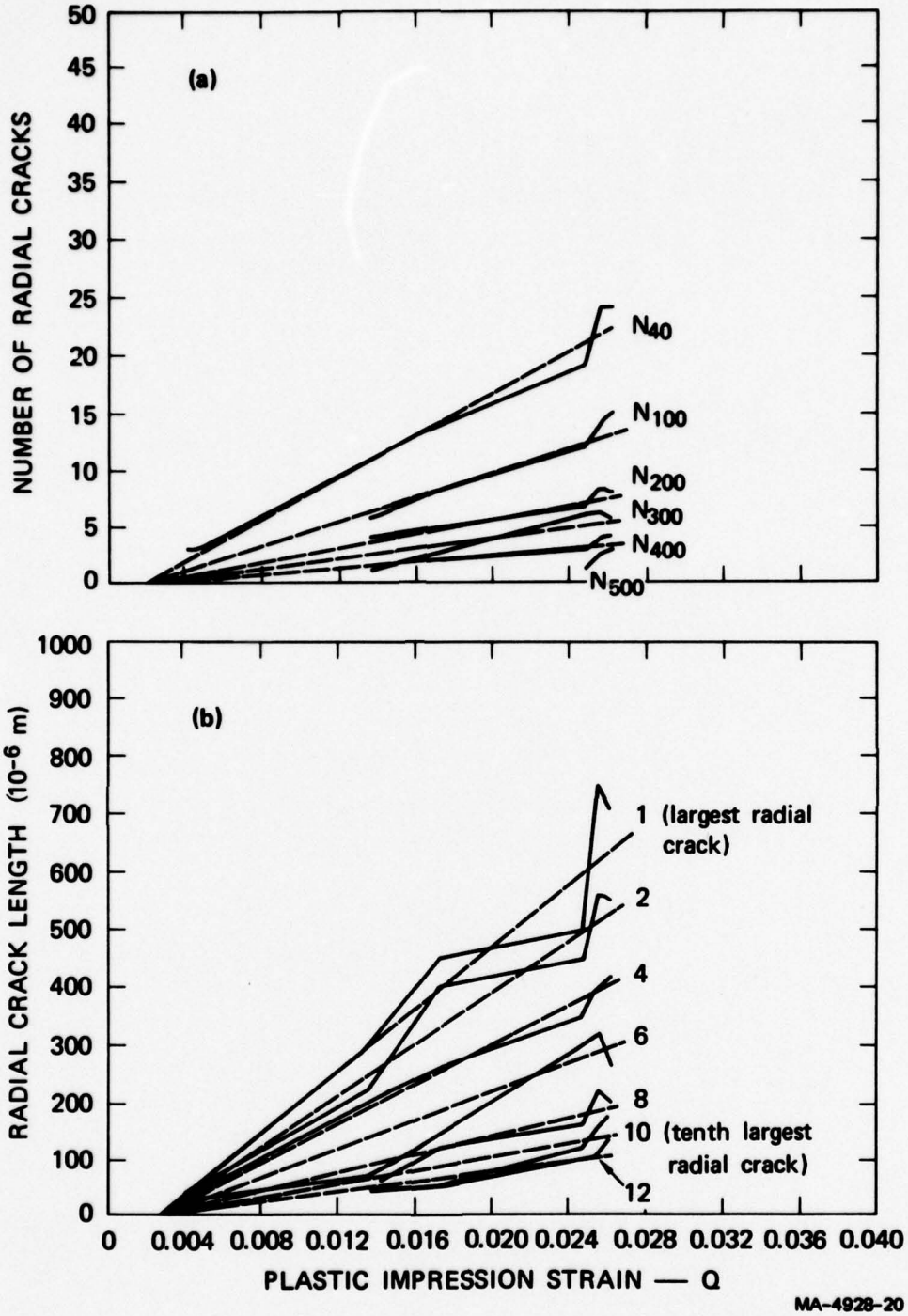

FIGURE 15 VARIATION OF NUMBER (a) AND SIZE (b) OF RADIAL CRACKS WITH PLASTIC IMPRESSION STRAIN FOR DOMINANT RADIALS PRODUCED BY IMPACTING 400-μm-DIAMETER SPHERES

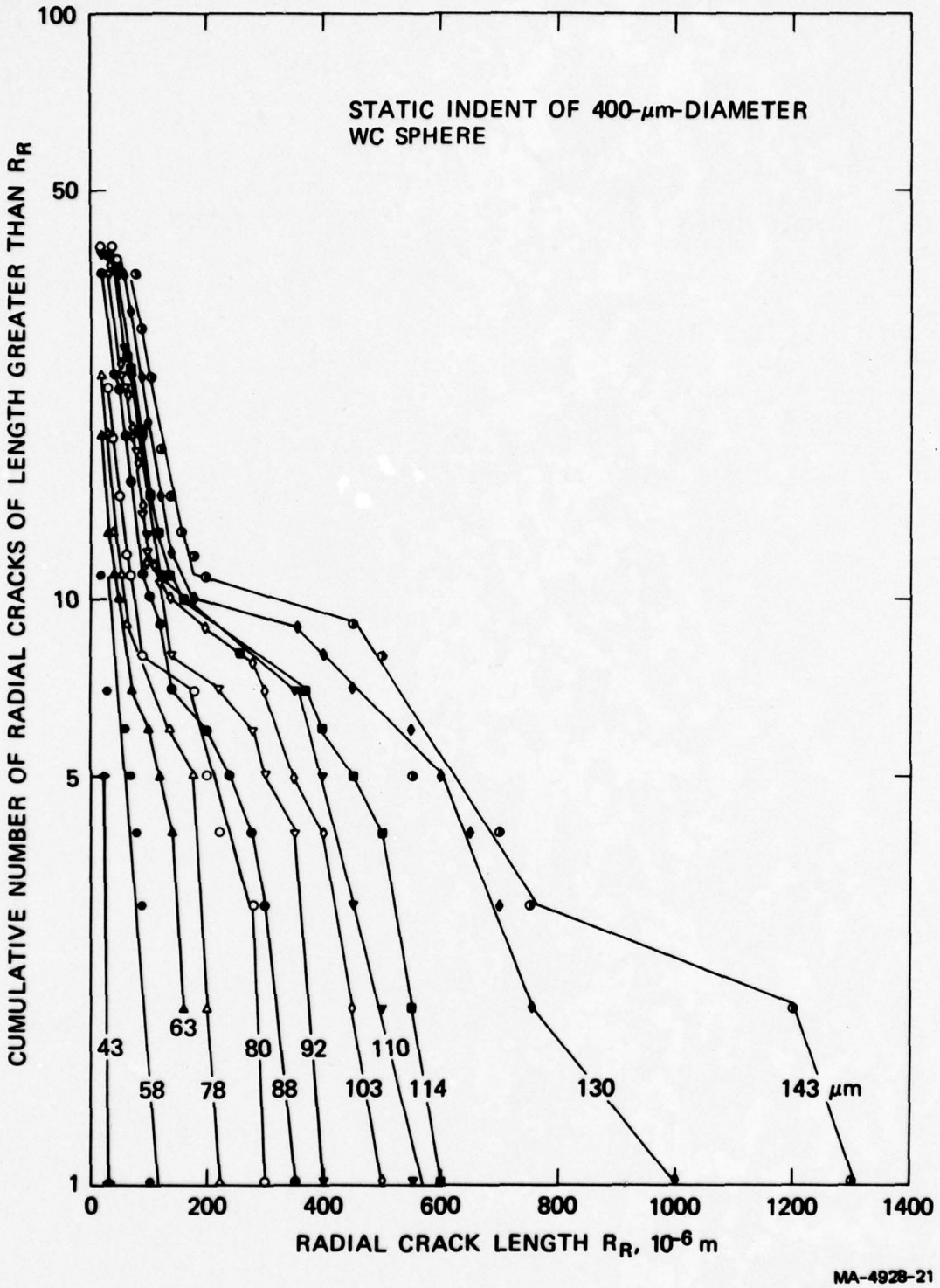

FIGURE 16 MEASURED SIZE DISTRIBUTIONS OF RADIAL CRACKS PRODUCED BY 400-μm-DIAMETER WC SPHERES UNDER VARIOUS INDENTATION LOADS

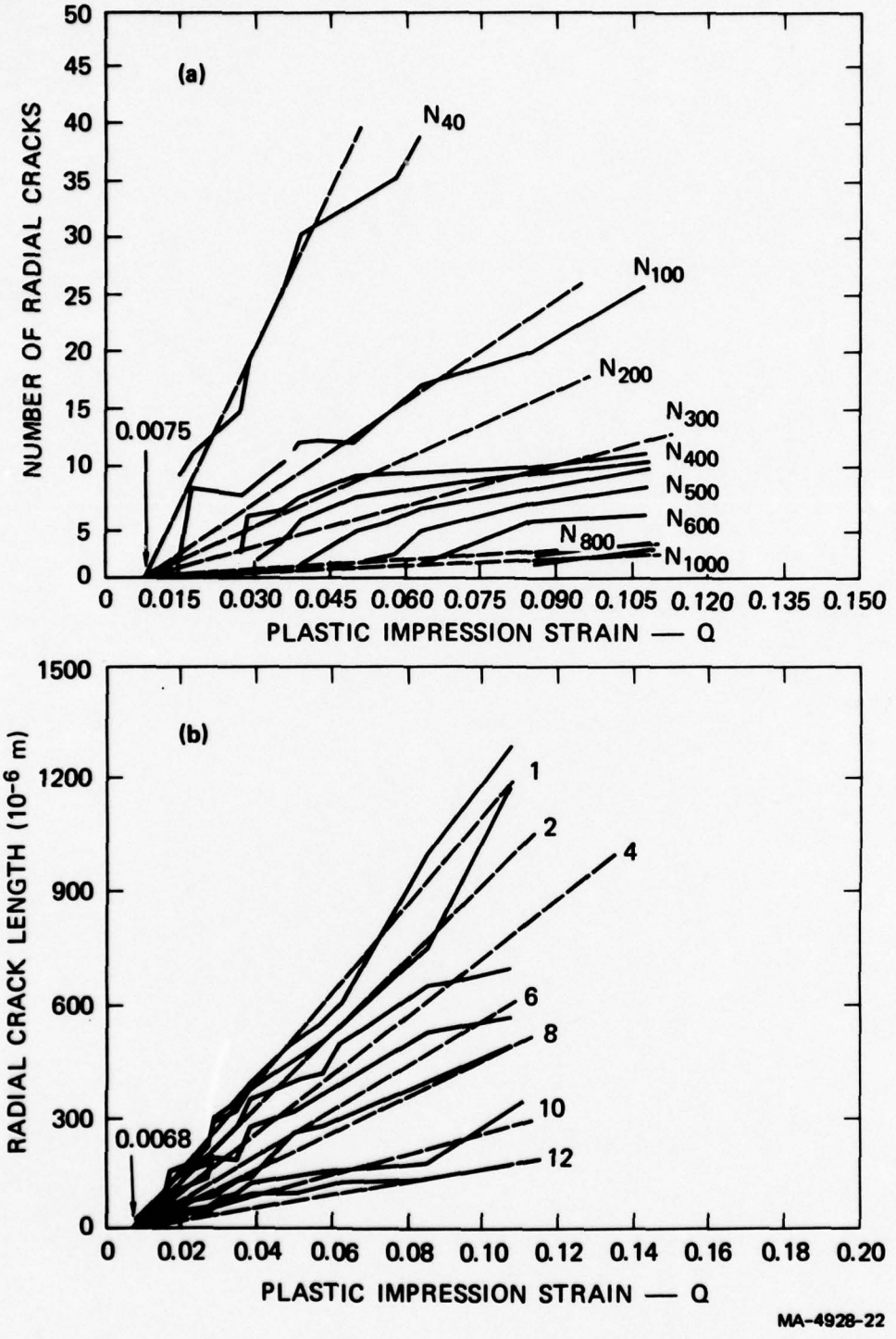

FIGURE 17 VARIATION OF NUMBER (a) AND SIZE (b) OF RADIAL CRACKS WITH PLASTIC IMPRESSION STRAIN FOR DOMINANT RADIALS PRODUCED BY QUASI-STATIC INDENTATION OF 400-μm-DIAMETER SPHERES

Particle Shape Effects

We began to investigate the effect of particle shape on impact damage by performing impact experiments using 800-μm-diameter by 1200-μm-long and 400-μm-diameter by 800-μm-long right circular cylinders made of hardened steel. Significant yaw of the projectile occurred in all experiments and resulted in nonsymmetric plastic impressions, Figure 18. The radial cracking pattern, however, was qualitatively similar to that produced by the sphere impacts. This suggests that the analysis developed for spherical particle damage can be applied for a cylindrical or an irregularly shaped particle if some representative measure of the plastic impression strain (perhaps the depth of the plastic impression) can be obtained. Alternatively, a correlation with impact velocity could be attempted.

Quasi-static indentation experiments were also performed using right circular cylinders of 800- and 400-μm diameters. Here yaw was not a problem, and crack distributions about symmetric plastic impressions (see inset in Figure 19) were determined and plotted as shown in Figures 19 and 20, using indentation load as a parameter. Comparison of these curves with those obtained from experiments with spherical particles shows that radial fracture behavior is similar: that is, the cracks initially exhibit an exponential distribution that increases with increasing load, and later 5 to 10 dominant radials break from the distribution and grow much larger. Extraction of crack nucleation and growth parameters from these data was not undertaken. It remains a subject for future work.

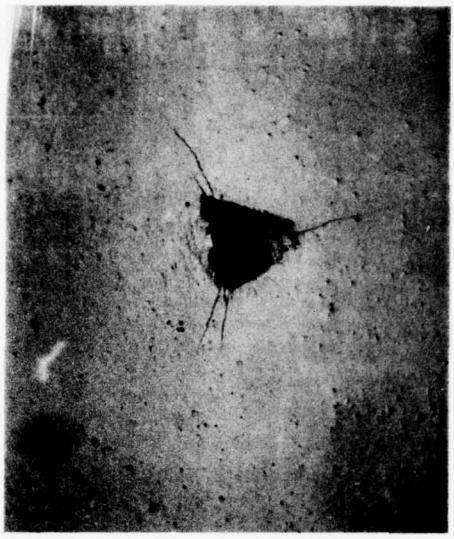

~ 18 m/s

~ 78 m/s

MP-4928-23

FIGURE 18 SURFACE DAMAGE PRODUCED BY 800-μm-DIAMETER RIGHT CIRCULAR CYLINDERS IMPACTING AT SEVERAL VELOCITIES

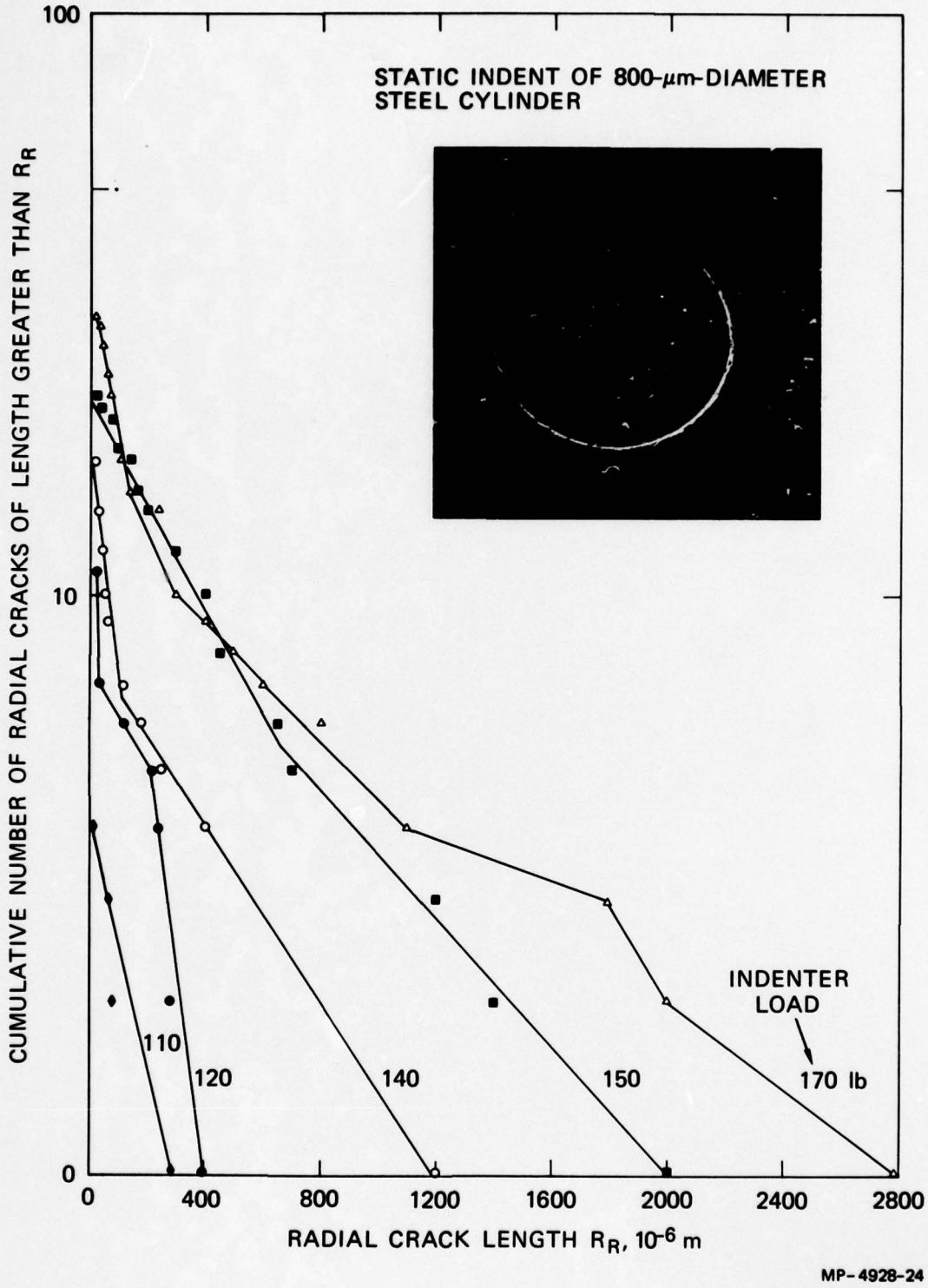

FIGURE 19 MEASURED SIZE DISTRIBUTIONS OF RADIAL CRACKS PRODUCED BY 800-μm-DIAMETER RIGHT CIRCULAR CYLINDERS UNDER VARIOUS INDENTATION LOADS

Insert shows plastic impression and radial cracks.

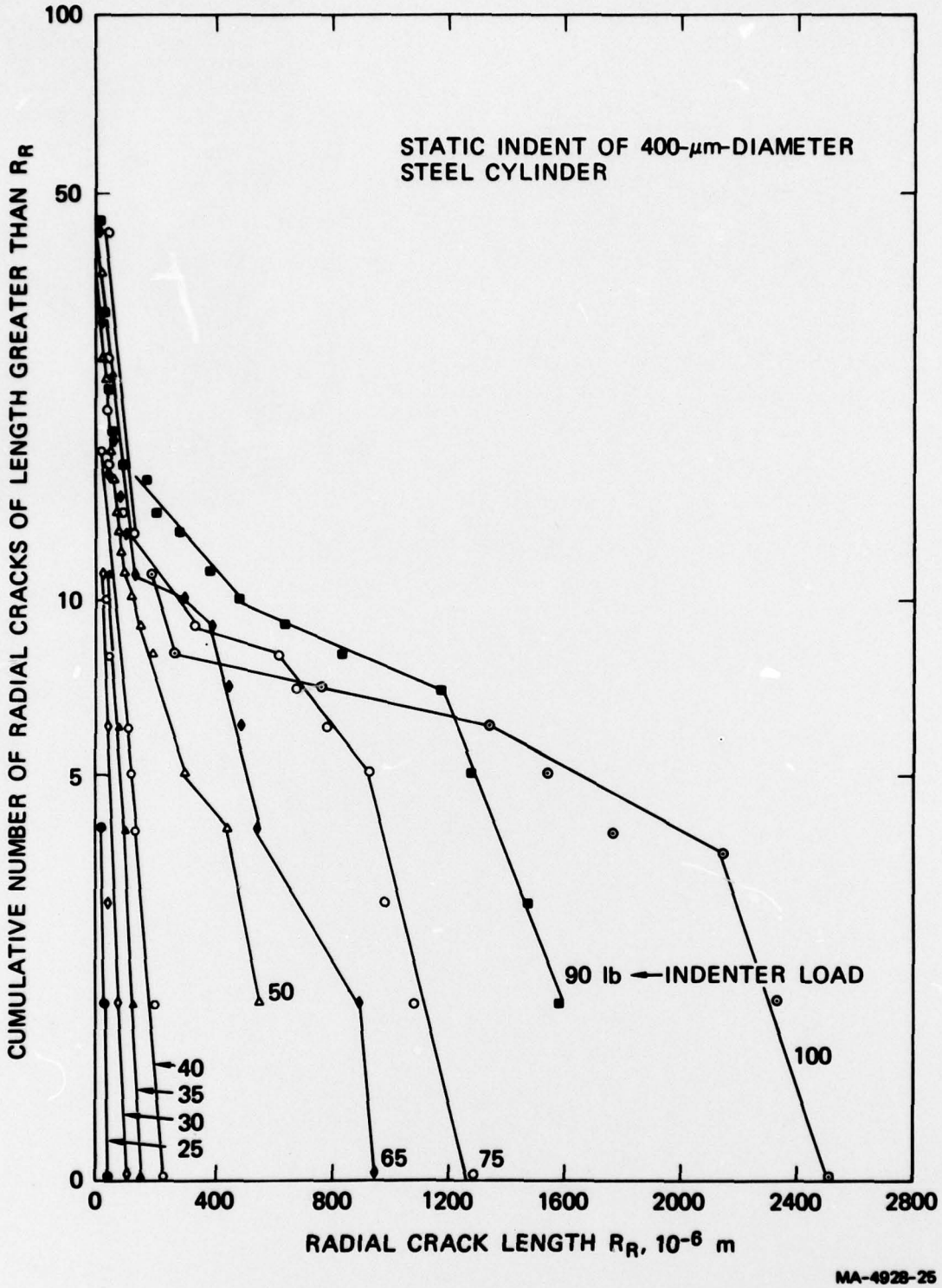

FIGURE 20 MEASURED SIZE DISTRIBUTIONS OF RADIAL CRACKS PRODUCED BY 400-μm-DIAMETER RIGHT CIRCULAR CYLINDERS UNDER VARIOUS INDENTATION LOADS

V DISCUSSION

Summary of Impact Damage Parameters

The parameters extracted from the particle damage analysis are summarized in Table 1. The values obtained from the impact and indentation experiments and from experiments with 400-μm and 800-μm-diameter spheres were compared to infer the effects of loading rate and particle size on particle-induced damage.

Rate effects for the 800-μm spheres seem to be small. Essentially no changes were observed in any of the damage parameters except the growth rate, where a 10% to 30% greater value was obtained under impact conditions. Substantial rate effects, however, were found in the 400-μm-sphere results where intercept strains for crack nucleation and growth under static loads were 4 to 5 times higher than for impact loads, and growth rates were roughly halved. Thus the importance of rate effects is not well established. Larger diameter particles indicate little rate effect, whereas smaller particles show substantial effects. Additional experiments are required to either reconcile or explain these observations.

The parameters in Table 1 provide a more consistent picture of size effects. A twofold change in particle dimension caused roughly a threefold change in values of all parameters. Thus the present results suggest that the extent of radial cracking about a particle impact site is considerably more sensitive to particle size than to loading rate.

An attempt was made to obtain size-independent crack growth parameters by normalizing with particle radius. The results are presented in the final two rows of Table 1. Although the values converged somewhat, considerable variation remains. The reason normalizing (replica scaling) did not bring the values into close agreement may be that the stress intensity factor in the vicinity of a static, elastic

Table 1

SUMMARY OF NUCLEATION AND GROWTH PARAMETERS
FOR RADIAL CRACKS PRODUCED IN CVD ZnS
BY IMPACT AND BY INDENTATION OF WC SPHERES

	800-μm-dia Sphere		400 μm-dia Sphere	
	Impact	Indent	Impact	Indent
Nucleation intercept strain, Q_i	0.18%	0.16%	0.20%	0.75%
Nucleation saturation strain, Q_{sat}	2.8%	2.8%	7.8%	8.8%
Rate of crack nucleation, B	390	380	130	120
Growth intercept strain, Q_o	0.14%	0.14%	0.26%	0.68%
Growth rate parameter, b				
Maximum	54 mm	48 mm	27 mm	12 mm
Average	42 mm	29 mm	17 mm	8 mm
Normalized growth rate parameter, b/r				
Maximum	130	120	130	60
Average	100	73	85	40

crack varies as the square root of the crack size. Thus, if fracture toughness (the critical stress intensity factor) governs the crack extension, we can expect less crack growth around smaller spheres. However, attempts to use toughness scaling did not improve the correlation significantly, and in any event cannot account for the agreement given by replica scaling between the 800-μm and 400-μm dynamic results. It can also be argued that the stress field gradient caused by geometrical divergence outweighs the effect of variation of stress intensity factor, particularly in the dynamic case.

To resolve these problems, it will be necessary to perform more experiments to improve the statistical data base and to perform more complete calculations of the load histories for the dynamic and static case. At the moment, however, the qualitative and quantitative comparisons of static and dynamic fracture damage suggest that the pertinent material properties describing impact damage may be obtainable largely from static indentation experiments.

Inferences from the Crack Size Distributions

The crack size distribution curves obtained in this work provide useful insight into the distribution of inherent flaws and the kinetics of crack nucleation and growth. In the following paragraphs we (1) deduce the inherent flaw size distribution and present the Batdorf argument to show that the distribution can be derived from simple probability theory and (2) deduce the form of the growth law from the shapes of the crack size distribution curves by analogy to shapes produced by application of elastic growth laws.

Crack Nucleation Sites in ZnS. Scientists have long attempted to identify the weak spots in a solid at which fracture initiates and leads to failure of a specimen or component. Microscopic examination of fracture surfaces or cross sections of partially failed specimens have often verified the presence of a heterogeneity at the origin of a crack that has apparently magnified the applied stress in a local volume of material and led to failure. Examples of such stress raisers are

inclusions and second-phase particles, pores, voids and cracks, and grain boundaries and grain boundary triple points.

A limited microscopic study of the microstructure of the CVD ZnS stock used in this program showed little evidence of inclusions, second phase particles, pores, voids, or cracks. The main microstructural heterogeneity appeared to be the crystallographic misorientations between neighboring grains and between colonies of grains, Figure 1 (b) and (c). However, examination of fracture surfaces in the scanning electron microscope could not confirm crack initiation at grain or colony boundaries.

Although we were not able to conclusively identify microstructural features at which fractures nucleated, we were able to deduce considerable information about their numbers and sizes. At low impact velocities and under low indenter loads, we observed exponential crack size distributions; i.e., we obtained linear curves in the log-linear space (Figures 7, 11, 14, 16, 19, and 20). This implies that the inherent flaw size distribution is also exponential and may be described by an equation of the form

$$N_g = N_o \exp\ (-R/R_i) \qquad (3)$$

where N_g is the number of flaws having a radius greater than R, N_o is the total number of flaws, and R_i is a parameter of the distribution. A similar expression with different values for N_o and R_i would describe the initial crack size distributions we observed.

These crack size distribution results are consistent with our observations in a wide variety of materials under both quasi-static and dynamic loads of exponential distributions of inherent flaws[4] and inclusions[5], stress-induced cracks and voids[6], and fragments[7]. McClintock[8] and Batdorf[9] have suggest why an exponential distribution is so ubiquitous in nature.

We quote from Batdorf's analysis[9] of penny-shaped cracks based on McClintock's assumption that cracks are random aggregations of unbonded grain boundaries:

> If q is the probability that a given boundary is unbonded, then q is also the probability that a crack with a length equal to one or more grain diameters exists at that location. The probability that two adjacent grain boundaries are cracked is q^2. This is also the probability that, at a given grain location, there is a crack two grains long or longer. Generalizing, the probability P(n) of a crack encompassing n or more adjacent grain boundaries is given by

$$P(n) = q^n = \exp(n \ln q) - \exp\{-\ln(q^{-1})n\}. \tag{4}$$

> Because n is proportional to crack length for a linear crack, eq. (4) implies a crack probability decreasing exponentially with length as noted previously by McClintock.
>
> In the case of a penny-shaped crack of radius c, the number of adjacent grains forming the crack is

$$n = \pi c^2/A_o, \tag{5}$$

> where A_o is the area of a single grain. Substituting eq. (5) into eq. (4), we obtain for the probability that the radius will exceed c,

$$p(c) = \exp\{-\ln(q^{-1})\ \pi\ c^2/A_o\}. \tag{6}$$

If we multiple P(c) by the total number of cracks per unit volume, N_o, and redefine c as R, we obtain equation (3) for the McClintock formula (4), with

$$R_1 = r/\ln(q^{-1}) \tag{7}$$

where r is the constant grain radius. Batdorf's formula (5) yields

$$N_g(R) = N_o \exp(-R^2/R_1^2) \quad , \tag{8}$$

with $$R_1 = r/[\ln(q^{-1})]^{\frac{1}{2}} \quad . \tag{9}$$

Since penny-shaped flaws seem more prevalent than linear ones, the above derivation suggests that equation (8) should describe experimental flaw distributions better than equation (3). Of course, over a limited size range, either form can be made to fit. The main point is that equations (3) or (8) can be derived from simple probability theory. Thus, despite our inability to identify or observe crack initiation sites, we are able to infer their size distribution quantitatively.

Crack Growth Behavior. The initial exponential distribution of crack sizes is not maintained at higher impact velocities and indenter loads, as is apparent in Figures 7, 11, 14, 16, 19, and 20. The initially linear curves in ln N vs R space develop a knee as five to ten dominant radials increase in length at a much faster rate than the other radials. The shapes of these curves reflect the growth characteristics of the cracks, and we attempted, by analogy to various time-dependent growth laws, to deduce a strain-dependent growth law describing the present data.

The size distributions in Figures 7, 11, 14, 16, 19, and 20 indicate two distinct growth behaviors. The smaller cracks (up to the 10th largest) maintain roughly an exponential size distribution with increasing plastic impression radius; i.e., the ln N vs R curve stays roughly linear. This behavior, with time rather than plastic impression radius as the parameter, is well described by a viscous growth law of the form

$$\dot{R} = A'R \tag{10}$$

which allows larger cracks to grow more than smaller cracks, and in such a way that an exponential distribution is maintained. Figure 21 shows the effect on an initially exponential distribution, and hence the appropriateness of the form of equation (10) to describe the observed behavior of small radial cracks. By analogy then we suggest

$$\frac{dR}{dQ} = AR \tag{11}$$

as the growth law for small radial cracks, where A is a growth coefficient.

A still better fit to the data is obtained if crack nucleation is allowed to occur with increasing plastic impression strain. The effect is to cause a slight upward curvature in the crack size distribution, Figure 21, a trend that is apparent in Figures 7, 11, 14, 16, 19, and 20.

The growth behavior of the five to ten largest cracks must be described by a quite different law. To deduce this law, we noted again the similarity between the experimentally determined crack size distribution curves and the shapes of distributions produced by various time-dependent laws. The simplest growth law, $\dot{R} = V_T$, which states that cracks grow at some constant velocity V_T (usually chosen to be a wave velocity), simply translates the distribution to larger sizes. Other elastic growth laws, obtained from energy balances by Mott[10], Dulaney and Brace[11], and Berry[12] and having the form $\dot{R} = V_T(1 - R^*/R)^n$ result in a concave downward shape reminiscent of the shapes obtained in our figures. Figure 22 shows the effect of these elastic growth laws on an initial exponential crack size distribution. (In creating this figure we have assumed for simplicity that no additional cracks nucleate and that, consistent with fracture mechanics concepts, cracks having radius less than R* do not grow.)

By analogy again, a growth law of the form

$$\frac{dR}{dQ} = \left(\frac{dR}{dQ}\right)_{max} (1 - R^*/R)^{1/2} \tag{12}$$

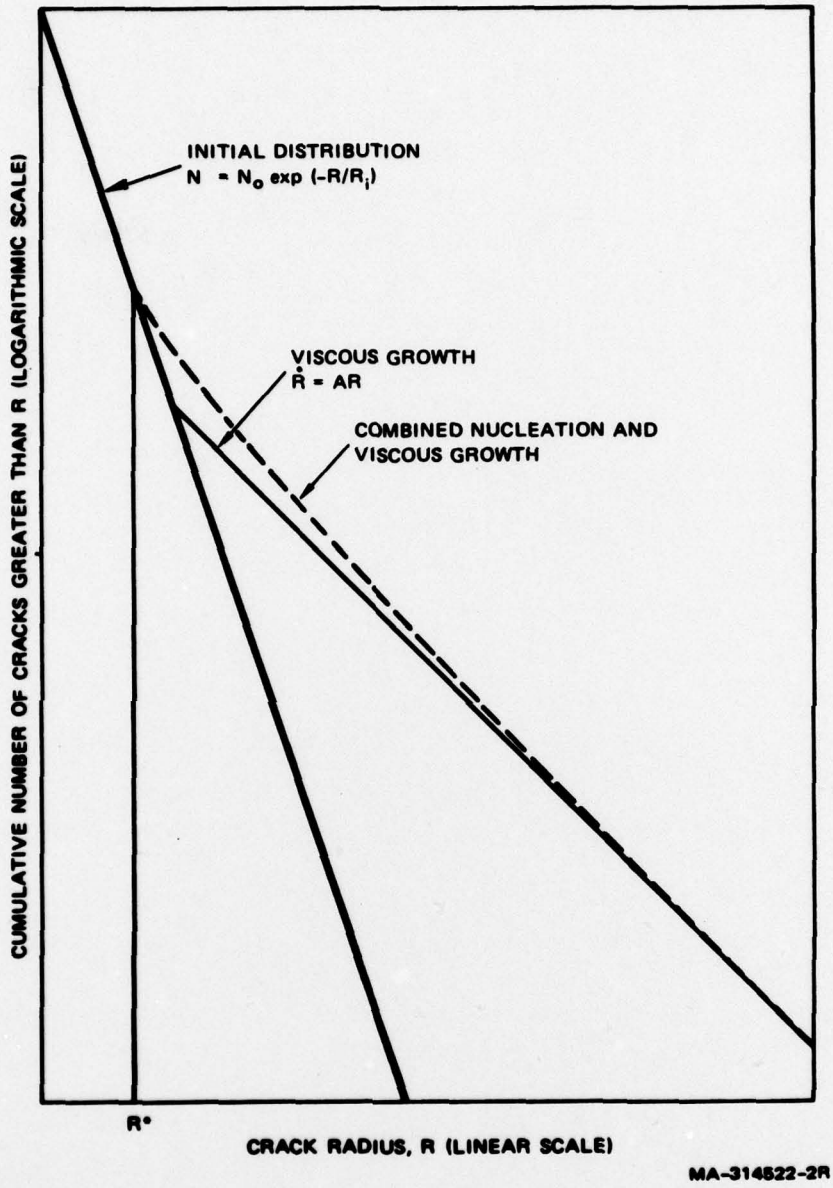

FIGURE 21 CRACK SIZE DISTRIBUTIONS PRODUCED BY GROWTH FROM AN INITIAL EXPONENTIAL DISTRIBUTION ACCORDING A VISCOUS GROWTH LAW

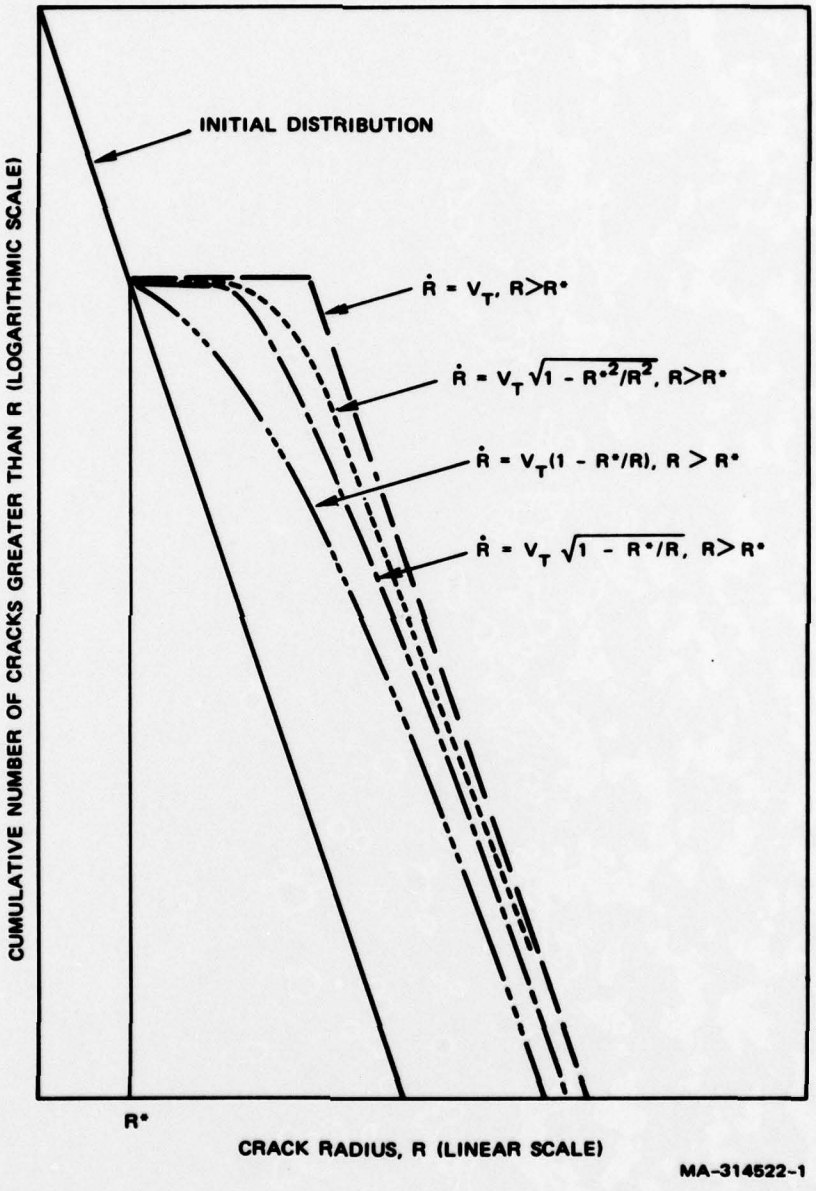

FIGURE 22 CRACK SIZE DISTRIBUTIONS RESULTING FROM SEVERAL ELASTIC GROWTH LAWS

is suggested for the dominant radial cracks, where $\left(\frac{dR}{dQ}\right)_{max}$ is a growth coefficient and the critical flaw size R* corresponds to the break in the ln N vs R curve. We note that determination of R*, a knowledge of the stress field in the vicinity of the impact or indent site, and the appropriate stress intensity calibration formula are the prerequisites for calculating dynamic and quasi-static fracture toughness.

VI RECOMMENDATIONS

The approach taken in this research program shows promise for providing a means to identify and evaluate material properties governing erosion behavior in ceramics. This approach should be further developed by the following research.

To establish the importance of rate effects, the impact and indentation results with 400-μm-diameter spheres should be checked in additional experiments.

Experiments with 200-, 1200-, and 2400-μm-diameter tungsten carbide spheres would be useful in indicating the scalability of the NAG parameters and in helping to define their limits of applicability.* The results will indicate if normalization of damage behavior is possible, and if so, if the data can be used to determine the appropriate scaling factor. Experiments with larger and smaller spheres would be helpful in sorting out rate effects from size effects.

Erosion equations proposed by other investigators should be applied to the extensive data base generated in this work to test the predictive abilities of the equations and to seek relationships between NAG parameters and more standard properties. Such relationships will help establish the role of macroproperties in determining impact fracture behavior and the extent of particle impact damage, and should also be useful in guiding the development of more impact-resistant microstructures. Impact and indentation experiments on other ceramics or differently processed ceramics would also aid in finding connections between erosion parameters and conventional properties.

---

*We expect that spheres above a certain radius will produce a change in fracture morphology from radial cracks to ring and cone cracks.[13]

The influence of particle properties should be investigated by performing impact experiments using spheres of other materials such as glass, nylon, Al_2O_3, and steel. Substantial evidence indicates that stress duration as well as stress amplitude determines fracture behavior under impact conditions; therefore, the acoustic impedance of the impacting particle should influence the observed damage and hence the NAG parameters.

Load parameters should be sought that are more suitable than plastic impression strain for correlation with impact damage. An approximate* description of the stress and strain field history in the vicinity of the impact site may help in identifying a simple, but effective, variable for correlating crack numbers and sizes.

Several of these suggested research tasks will be performed in the next year under the current contract.

*Determination of the stress and strain field history in the vicinity of an impact site is a formidable task when both plastic flow and fracture are occurring.

REFERENCES

1. D. A. Shockey, D. J. Rowcliffe, and K. C. Dao, "Fracture Toughness of CVD ZnS," Topical Report for Office of Naval Research on Contract N00014-76-C-0657, SRI International (March 1977).

2. A. G. Evans and T. R. Wilshaw, "Quasistatic Solid Particle Damage in Brittle Solids - I. Observations, Analysis and Implications" Acta Met. 24 939-965 (1976).

3. A. G. Evans and T. R. Wilshaw, "Dynamic Solid Particle Damage in Brittle Materials: An appraisal," J. Mat. Sci., 12, 97-116 (1977).

4. D. A. Shockey, D. R. Curran, L. Seaman, J. T. Rosenberg, and C. F. Petersen, "Fragmentation of Rock Under Dynamic Loads," Int. J. Rock, Mech. Sci., & Geomech. Abstr., 11, 303-317 (1974).

5. D. A. Shockey, L. Seaman, K. C. Dao, and D. R. Curran, "A Computational Model for Fracture of Pressure Vessel Steel Derived from Experimental Data," ASME Paper No. 78-PVP-92 (1978).

6. D. R. Curran, L. Seaman, and D. A. Shockey, "Dynamic Failure of Solids," Physics Today 30, 46 (January 1977).

7. D. C. Erlich, L. Seaman, D. A. Shockey, and D. R. Curran, "Development and Application of a Computational Shear Band Model," Final Technical Report on Contract DAAD05-76-C-0762 to U.S. Army Ballistic Research Laboratory, Aberdeen, MD (1977).

8. F. A. McClintock, "Statistics of Brittle Fracture" in Fracture Mechanics of Ceramics, Vol. 1, R. C. Bradt, D.P.H. Hasselman, and F. F. Lange, Eds. (Plenum Press, New York 1973), pp. 93-114.

9. S. B. Batdorf, Nuc. Eng. Design, 35, 349 (1975).

10. N. F. Mott, "Fracture of Metals: Some Theoretical Considerations," Engineering, 165 , 16 (1948).

11. E. N. Dulaney and W. F. Brace, "Velocity Behavior of a Growing Crack," J. Appl. Phys., 31, 2233 (1960).

12. J. P. Berry, "Some Kinetic Considerations of the Griffith Criterion for Fracture," J. Mech. Phys. Solids, 8, 194-216 (1960).

13. B. R. Lawn and D. B Marshall "Indentation Fracture and Strength Degradation in Ceramics" in Fracture Mechanics of Ceramics, Vol. 3, R. C. Bradt, D.P.M. Hasselman, and F. F. Lange, Eds. (Plenum Press, New York, 1978), pp. 205-230.